energies

Article

Complex Positioning System for the Control and Visualization of Photovoltaic Systems

Filip Žemla *, Ján Cigánek, Danica Rosinová, Erik Kučera and Oto Haffner

Faculty of Electrical Engineering and Information Technology, Slovak University of Technology in Bratislava, 841 04 Bratislava, Slovakia; jan.ciganek@stuba.sk (J.C.)
* Correspondence: filip.zemla@stuba.sk

Abstract: This paper presents a proposal of a complex mechatronic system that enhances the effectivity of obtaining energy from renewable resources. The main focus is on the photovoltaic energy system, which obtains electricity from the conversion of solar radiation through photovoltaic crystalline silicon-based panels. The design of the complex mechatronic system consists of several steps. The structural design of the photovoltaic panel positioning unit in the form of a three-dimensional model is made in the selected modelling programming environment. Subsequently, a propulsion system is proposed for the designed structure, the functionality of which is verified in the programming environment Automated Dynamic Analysis of Mechanical Systems. The control system design using a programmable logical controller is also presented. The corresponding control algorithm is designed in the programming environment Step7 and covers the optimal positioning of photovoltaic panels. The developed application in the WinCC environment provides a visualization of the positioning control process. The conclusion is devoted to the assessment of the obtained results for the proposed complex mechatronic system for photovoltaic panel positioning in comparison with photovoltaic panels in fixed installation. The presented results were obtained by simulations.

Keywords: mechatronic systems; visualization; control systems; energy systems; photovoltaic panels; programmable logical controller (PLC); supervisory control and data acquisition (SCADA) systems

Citation: Žemla, F.; Cigánek, J.; Rosinová, D.; Kučera, E.; Haffner, O. Complex Positioning System for the Control and Visualization of Photovoltaic Systems. *Energies* **2023**, *16*, 4001. https://doi.org/10.3390/en16104001

Academic Editor: Chunhua Liu

Received: 22 March 2023
Revised: 27 April 2023
Accepted: 3 May 2023
Published: 9 May 2023

1. Introduction

Today, few people can imagine everyday life without electricity, but few realize the significant environmental impact that its production has on the scope of our needs. Energy demands are constantly increasing, as evidenced by the projected increase in the current electricity consumption by 30–35% every decade. Considering the fact that approximately 2/3 of the world's production comes from the thermal conversion of non-renewable sources such as coal and natural gas, which are significant producers of greenhouse gases and CO_2 emissions, the negative impact on the environment is widely known. For several decades, only around 20% of the world's electricity production was obtained from renewable sources due to the geographical or climatic requirements, or due to the high production cost [1]. Over the past 10 years, this share has increased to almost 30% and can be expected to continue to grow. Therefore, it is extremely important to develop and improve the efficiency of these forms of obtaining electrical energy, which motivates the presented research involving the design of a complex mechatronic system for the control and monitoring of the production of electrical energy using a photovoltaic system. In the design, a monocrystalline panel is considered, because it achieves higher efficiency with optimal placement of the photovoltaic panel. Our solution focuses on the design of the positioning system and is not limited to this type of photovoltaic panels.

This paper deals with the positioning of photovoltaic panels (PV) in order to track the trajectory of the Sun's movement in the sky so that its rays fall on the surface of the panels at the best possible angle. Thus, higher efficiency in collecting solar energy is achieved.

At the same time, we have to design such a control system that its energy consumption is significantly lower than the benefit of collecting solar energy.

In work [2], several methods are available for tracking the Sun for the purpose of positioning photovoltaic panels. These methods are based on soft computing approaches and for this reason, they are significantly more computationally demanding than our proposed solution.

Several projects have been published that deal with more complex solutions for the PV placement and energy harvesting. Nevertheless, the positioning system can be further improved, which would increase generating electricity from solar power. In Table 1, several existing systems are summarized. From the overview of the projects, it can be observed that the efficiency of positioning systems for PV has been continuously improving over the past few decades.

Table 1. General results [3,4].

Algorithm References		Error	Gain in Energy Production Compared with a Non-tracking System
Closed-loop Control	Maish (1990) [5]	1°	-
	Enslin (1992) [6]	-	10–15%
	Brown et al. (1993) [7]	<0.01°	-
	Kalogirou (1996) [8]	0.05–0.2°	-
	Khalifa et al. (1998) [9]	-	75%
	Falbel et al. (2002) [10]	0.05°	-
	Al-Mohamad (2004) [11]	-	20%
	Abdallah (2004) [12]	-	15–44%
	Aiuchi et al. (2004) [13]	0.1°	-
Open-loop Control	Blanco-Muriel et al. (2001) [14]	0.08°	-
	Abdallah et al. (2004) [15]	-	41%
	Reda et al. (2004) [16]	0.0003°	-
	Chen F. et al. (2006) [17]	0.02°	-
	Chen F. et al. (2007) [18]	0.2°	-
	Grena (2008) [19]	0.0027°	-
	Chong et al. (2009) [20]	-	-

Compared to [21], we offer a much simpler calculation of the Sun’s trajectory during the day. The presented solution is comprehensive and includes the entire positioning system design methodology, from structural design, through control design, to visualization of the positioning process and statistical evaluation of energy collection.

In [22], the authors offered a solution without a positioning system, but achieved higher efficiency in energy collection when using additional mirrors compared to a fixed panel without mirrors by 53%. In a related work [23], the authors report an increase in efficiency by 6.8% using a positioning system. The positioning algorithm was supplemented with the values of added sensors such as a GPS module, magnetometer, RTC module, gyroscope and temperature and humidity sensor. The work does not mention a specific control system or its own consumption for positioning.

Positioning systems are available on the market, see e.g., [24,25]. Their price is around EUR 900 and they offer a 35–40% increase in electricity productivity. In [26], a review of recent results regarding the effectiveness of different solutions for the placement of PV systems is available. Most of the compared dual-axis systems show efficiencies in the range of 20–45% compared to fixed PV panels. Our solution aims to achieve higher efficiency at a comparable price of the construction, including the positioning system and its control.

This paper includes an analysis of the photovoltaic energy system, where the current state as well as trends in this area are considered. A large emphasis is put on the factors that affect the efficiency of energy conversion, especially for silicon panels. A complex mechatronic system is subsequently designed for these panels, ensuring the positioning of the photovoltaic panel directly at the Sun during the day, to maximize the efficiency of converting solar radiation into electrical energy. The work consists of the design of the mechanical structure (console) as well as the software solution for the PLC and the visualization of the proposed positioning. The conclusion of the work is devoted to the evaluation of the profit of the positioning of the photovoltaic panel compared to fixed oriented panels.

The main contribution of this paper can be summarized as the design and control of the photovoltaic panel positioning system, so that we can significantly increase the generated electrical energy when compared to a static photovoltaic system. The control considers the minimization of the energy consumption required for positioning the panel using a stepper motor. The development of a complex mechatronic system is based on co-simulation, as follows: Automated Dynamic Analysis of Mechanical Systems (MSC Adams)–physical model of construction, PV and stepper motors; MATLAB Simulink–simulation of shaft positioning. A partial task is the design of a specific stepper motor and its parameters. The verification of the proposed design is achieved by a simulation experiment comparing the net energy gained from the designed photovoltaic system and from the fixed photovoltaic system.

This contribution is focused on the design of the simple construction that meets the specified requirements for robustness, stability, accuracy and resistance to external influences, as well on the design of the control system for positioning the photovoltaic panel with minimum consumption to maximize the gain of the generated electrical energy.

2. Problem Formulation and Preliminaries

Since the work deals with the photovoltaic energy system, in this section, we recall the corresponding physical background and take a closer look at photovoltaic cells and positioning systems.

2.1. Photovoltaics—Theoretical Background

Mankind has been interested in photovoltaics, or the conversion of solar radiation into electrical energy, since an important discovery was made in 1839 by the French physicist Alexandre Edmond Becquerel, who observed the interaction of solar radiation with chemical processes generating an electric current in an electric circuit consisting of liquids and metals [27]. Czochralski's method made it possible to create a semiconductor PN junction, based on which the first photovoltaic silicon cell with an efficiency of 4.5% was produced in 1954 [28]. In the following years, production technologies began to improve as well as experiments with new materials in order to increase the low efficiency of converting solar energy into electricity. The developments reached photovoltaic cells with an efficiency of 44% in laboratory conditions [29].

Photovoltaics, with its long history, is still experiencing its greatest boom today thanks to modern technologies that have allowed for a reduction in the production price of photovoltaic panels and mainly due to the growing pressure to protect the environment. The intense development in this area brings a constant supply of innovations with increasing conversion efficiency, which makes photovoltaics increasingly lucrative in the field of renewable energy sources. This is evidenced by the worldwide annual increase of 30% in the installed capacity of power plants that use solar radiation to produce electricity [30].

Solar energy spreads from the Sun continuously in all directions through space, decreasing with the distance that solar energy has to travel; therefore, the energy falling on the Earth's atmosphere is only a small fraction of the generated energy. The intensity falling on the Earth's atmosphere can be expressed by (1), where the total solar radiation H_{sun} is obtained from the Stefan–Boltzmann law on the thermal radiation of bodies (2), which is the product of the Stefan–Boltzmann constant and the bodies' absolute temperature. When calculating the radiation intensity, we multiply the total solar radiation by the area of the

Sun and divide this by the area over which the solar radiation extends at the distance of our globe. The calculation is illustrated in Figure 1 [31,32].

$$H_0 = \frac{4\pi R_{sun}^2}{4\pi D^2} H_{sun} = \frac{R_{sun}^2}{D^2} H_{sun}, \tag{1}$$

$$\text{where } H_{sun} = \sigma T^4, \tag{2}$$

in which: σ—Stefan–Boltzman constant [$\frac{\mathrm{W}}{\mathrm{m^2K^4}}$]; T—absolute temperature [K]; H_{sun}—intensity of radiation on the surface of the Sun [$\frac{\mathrm{W}}{\mathrm{m^2}}$]; R_{sun}—radius of the Sun [m]; D—Earth distance from the Sun [m]; H_0—radiation intensity at a given distance [$\frac{\mathrm{W}}{\mathrm{m^2}}$].

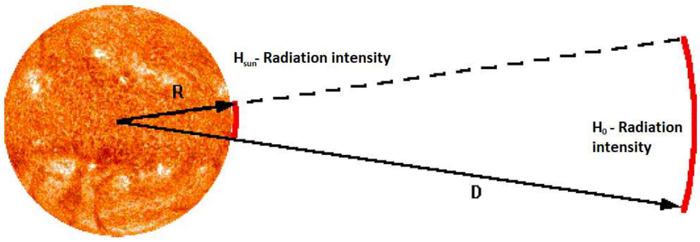

Figure 1. Spreading the intensity of solar radiation [33].

Substituting the distance between the Earth and the Sun into Equation (1), we can obtain the value of the solar constant H_{const} = 1353 kW/m^2, which indicates the intensity of solar radiation falling on the Earth's atmosphere [32]. The solar constant is generally used for photovoltaic calculations, but the actual value of the solar intensity falling on the surface of the Earth's atmosphere is variable during the year, since the trajectory of the Earth's orbit around the Sun is an ellipse. The elliptical trajectory causes the value of the actual radiation intensity to vary in the range of 3.4% of the solar constant, while it reaches its maximum in January, and the value can be expressed using (3). Based on this equation, we can calculate the value of the incident radiation intensity on the upper layer of the atmosphere for a given day of the year n [34,35].

$$H = H_{const}\left(1 + 0.033\cos\left(\frac{360(n-2)}{365}\right)\right), \tag{3}$$

in which: H—radiation intensity [$\frac{\mathrm{W}}{\mathrm{m^2}}$]; H_{const}—solar constant [$\frac{\mathrm{W}}{\mathrm{m^2}}$]; n—day of the year.

Solar radiation falls on the Earth's surface after radiation from the solar core, traveling through space and through the Earth's atmosphere in the following three forms: direct, diffuse and reflected solar radiation. The reflected component is very limited in nature, as far as the Earth's surface is concerned, but this value can be slightly higher in the case of water bodies, and in the case of populated areas where reflections occur from, for example, buildings. Nevertheless, the use of this component for the benefit of a photovoltaic power plant is quite problematic [36].

Photovoltaic power plants on the Earth's surface mainly use direct sunlight and diffuse radiation. The main production component is direct sunlight, but the diffuse component makes up a significant part of the production and in some cases, it even exceeds the gain from direct sunlight. For example, in Central Europe, with fixed-oriented panels, production from the diffuse component with a 90% share in global radiation prevails in the winter period. In annual averages, it ranges between 50 and 70% of global radiation, while the term global radiation refers to the sum of direct and diffuse solar radiation [36,37].

However, it should be remembered that the density of the energy flow on the Sun's mantle is around 63 MW/m^2. At the boundary of the Earth's atmosphere, it reaches a value of around 1366 kW/m^2, and after passing through the atmosphere to the Earth's surface under ideal conditions, solar radiation reaches an energy density of up to 1 kW/m^2 [34]. However, if we look at this on a global scale, 18×10^{16} W of solar energy falls on the

Earth under favourable conditions [38,39]. Since the Sun is about halfway through its life cycle, which lasts 10 billion years, we can consider this resource as an inexhaustible, highly prospective and, above all, clean source of energy.

On average, around 3500 Wh/m^2 falls on the territory of the Slovak Republic per day and the difference in this value between northern and southern Slovakia varies slightly, up to 15% of global radiation and the maximum value is reached in southern Slovakia. In northern Slovakia, however, there are areas with local extremes in areas with high altitudes. In the annual summary, the global radiation falling on the territory of the Slovak Republic amounts to 1200–1350 kWh/m^2 per year (Figure 2). The values are determined based on measurements of meteorological stations in Slovakia over 15 years [40].

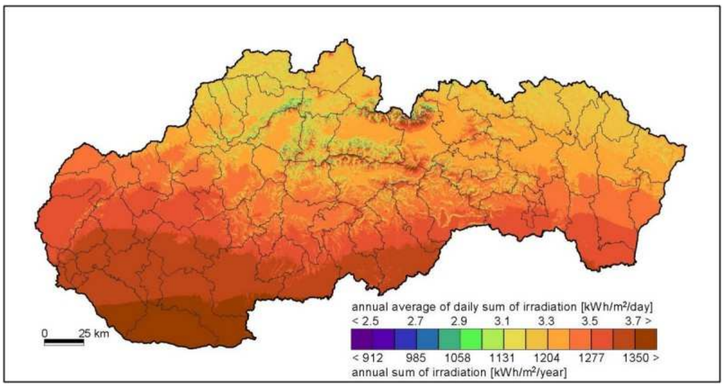

Figure 2. Solar radiation in the atmosphere on the territory of Slovak Republic [40].

For analysis in photovoltaics, however, knowledge of the measured average values of incident solar energy for a given period is not always sufficient, and it is necessary to calculate the influence of the atmosphere on the amount of incident solar energy. As we have discussed above, solar radiation when passing through the atmosphere is affected by various particles in the atmosphere. Their mutual interaction can be manifested either by absorption, reflection, or their subsequent emission. The calculations are based on the knowledge of the solar constant and the 30% fraction of absorption and scattering of solar radiation during the shortest path through the atmosphere, i.e., when the Sun is at its zenith [41,42].

The relative position of the Sun to the observer is variable in time, and thus the effective amount of atmosphere through which solar radiation passes also changes. The influence of this atmospheric mass is expressed by the AM coefficient, calculated on the basis of (4) [41]. Therefore, the angle from the zenith θ determines the angle at which the Sun is located from the zenith. The resulting atmospheric mass coefficient is, therefore, $AM = 1$ and if the angle from the zenith is $\theta = 0^\circ$ at the same time as the angle increases, the AM coefficient also increases [41].

$$AM = \frac{1}{\cos(\theta)}, \tag{4}$$

in which: θ—angle from the zenith [°].

However, for our needs in photovoltaic system design, it is necessary to know the intensity value of either direct or global radiation. This relationship is derived based on the knowledge of the solar constant H_{const} = 1.353 kW/m^2, the amount transferred by the atmosphere in the proportion of 70% and the empirical constant obtained by observations, which describes the inhomogeneity in the individual layers of the atmosphere and is equal to 0.678. Based on these data, using the coefficient of the atmospheric layer, we obtain an equation for calculating the intensity of direct solar radiation I_D (5) [34,42].

$$I_D = H_{const} 0.678^{\left(AM^{0.678}\right)}, \tag{5}$$

in which: AM—atmospheric mass coefficient.

It is obvious that with increasing altitude, the influence of the atmosphere will decrease, and the value of the solar intensity will increase. The effect of altitude is not significant in common ground photovoltaic systems and is, therefore, neglected in most calculations. However, if the investigated area is located at significantly higher altitudes, the real value of the solar radiation intensity could differ significantly. An empirical dimensionless constant obtained by measurements at a height of several kilometres above sea level (α = 0.14) is, therefore, added to the relationship; thus, the resulting (6) determines the value of the solar radiation intensity I_D with respect to the altitude h [43].

$$I_D = H_{const}\left[(1-\alpha h)0.678^{\left(AM^{0.678}\right)} + \alpha h\right], \tag{6}$$

in which: α—empirical constant equal to 0.14, h—altitude [km].

To determine the intensity of global radiation, it is also necessary to know the share of the diffuse radiation component and this value is usually equal to a value close to 10% of direct solar radiation. Calculation of global radiation intensity is, therefore, possible based on (7), assuming a cloudless day and impact on a vertically inclined plane [44].

$$I_G = 1.1 I_D, \tag{7}$$

in which: I_D—intensity of direct sunlight [$\frac{kW}{m^2}$].

The value of the intensity of the diffuse component of solar radiation can be determined more precisely based on more exact calculations that consider more parameters, but for the needs of this work, the value obtained from (7) is sufficient. Figure 3 shows the spectral power density of global radiation, i.e., its intensity for selected weights of atmospheric coefficients AM and the angle of incoming rays from the Sun to the Earth surface h [45,46].

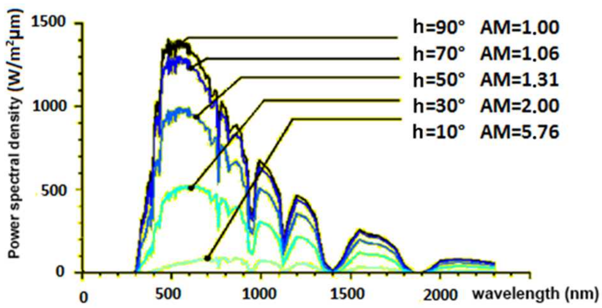

Figure 3. Solar radiation in the atmosphere on the territory of the Slovak Republic [40].

The incident electromagnetic radiation can be represented by a given wavelength and intensity or by the number of photons with energy W. A photon interprets a quantum of electromagnetic radiation, which represents a certain discrete amount of energy. So, electromagnetic radiation is a flow of photons carrying a finite amount of energy. Energy W can be expressed based on Planck's law [47].

$$W = hv = \frac{hc}{\lambda}. \tag{8}$$

in which: h—Planck's constant [J s]; v—radiation frequency [$\frac{1}{s}$]; c—speed of light [$\frac{m}{s}$]; λ—wavelength [µm].

Based on the width of the band gap W_G of the semiconductor material, the so-called absorption edge is defined, which determines the maximum wavelength of the incident radiation that the given semiconductor is able to absorb. For higher values of wavelengths, the energy of photons is no longer sufficient for absorption events and the given substance behaves as transparent. The range of wavelengths absorbed by a semiconductor can be expressed by (9). For silicon, the absorption edge is approximately λ_{MAX} = 1.1 µm [48].

$$\lambda \leq \frac{1.24}{W_G}, \tag{9}$$

in which: W_G—the width of the forbidden band [eV].

Based on the above relations, electromagnetic radiation will be absorbed in a semiconductor if its energy is higher than the band gap $W \geq W_G$. In addition to absorption, events such as spontaneous emission or stimulated emission can occur in semiconductors when interacting with electromagnetic radiation, as illustrated in Figure 4. Below, we consider only absorption for generating electrical energy based on the conversion from electromagnetic radiation. Spontaneous emission can, however, under certain circumstances occur in photovoltaic cells in the form of a non-radiative transition, when the energy released by the recombination of an electron from the conduction band with a hole in the valence band is sold to the crystal lattice in the form of thermal energy. However, this phenomenon is highly suppressed by the asymmetry of the PN junction. Stimulated emission is not essential for the needs of this work, so it will not be analyzed [49].

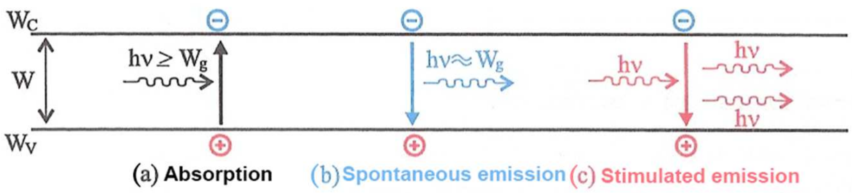

Figure 4. Interactive events [50].

The size of the energy barrier in the PN junction is given by the size of the diffusion voltage U_D. The size of the diffusion voltage is determined by the temperature and the concentration of acceptors and donors determined by the doping of the silicon structure with impurities. The resulting relationship for calculating the size of the diffusion stress U_D is given by (10) [51].

$$U_D = \frac{kT}{e} \ln\left(\frac{N_D N_A}{n_i^2}\right), \tag{10}$$

in which: k—Boltzmann's constant $[\frac{\mathrm{J}}{\mathrm{K}}]$; N_D—concentration of donors $[\frac{1}{\mathrm{m}^3}]$; N_A—concentration of acceptors $[\frac{1}{\mathrm{m}^3}]$; n_i—intrinsic concentration $[\frac{1}{\mathrm{m}^3}]$.

This description generally applies to semiconductor structures without external influences, i.e., without a connected external source or circuit, and also for our needs of photovoltaics in an unlit state. Through the interaction of the PN junction with the radiant flux and its influence on the energy levels, photons interact with the crystal structure, which is manifested by the generation of electron and hole pairs. Due to the energy barrier and electric potential at the space charge interface, these pairs are separated, and electrons can freely pass from the P layer to the N layer. However, if a pair is generated and subsequently splits in the N layer, this allows only an extremely small number of electrons to pass into the P layer. So, the consequence of illumination is an increase in the concentration of minor charge carriers. The difference between the Fermi levels during illumination is given by the potential difference, which corresponds to the photovoltaic voltage U_P. However, the size of the photovoltaic voltage cannot be greater than the difference of the original curvature of the energy levels, i.e., it cannot be greater than the diffusion voltage U_D. In practice, this means for silicon photovoltaic cells a value of around 0.6 V.

2.2. Photovoltaic Cells

The converters of solar energy into electrical one are based on physical principles. Photovoltaic cells of the first generation are based on crystalline silicon structures and a

P-N junction. Silicon in this generation is processed as monocrystalline or multi-crystalline. However, the absorption coefficient of silicon α determines the thickness of the semiconductor at least 100 μm for the given intensity of solar radiation to absorb the maximum incident energy. The calculation of the absorption thickness of the semiconductor is based on (11). From this fact, it follows that a relatively large amount of material in the form of crystalline silicon is required for the production of such photovoltaic cells, which is the reason why they are also called bulk photovoltaic cells [49–53].

$$E_{opt} = E_{0opt}\exp(-\alpha y), \tag{11}$$

in which: E_{opt}—intensity of radiation in a semiconductor $[\frac{W}{m^2}]$; E_{0opt}—ntensity of incident radiation $[\frac{W}{m^2}]$; α—absorption coefficient $[\frac{1}{m}]$; y—depth in semiconductor [m].

The structure of the photovoltaic cell is determined by the technological processing of silicon, while the technology of monocrystalline or multicrystalline processing is diametrically different. The production of a multicrystalline structure is significantly simpler and cheaper, which, however, is reflected in the slightly lower efficiency of the photovoltaic cell, but this difference is in the order of percent. The processing of monocrystalline silicon is significantly more demanding for technological equipment than the energy intensity of the production process. For both structures, as in semiconductor technology in general, a high purity of the material is necessary, which again makes the given process difficult and demanding, both financially as well as energetically, but research in this area has progressed and more innovative chemical processes for cleaning silicon are under development [54].

The most important step in the preparation of silicon structures is the creation of a P-N junction, which ensures the entire process of converting sunlight into electrical energy. The creation of the P-N junction was described earlier. The N-type semiconductor layer is created by the diffusion of phosphorus (P) and the diffusion is applied to the top layer of the silicon structures. The N-type layer created by diffusion is disproportionately smaller in width compared to the P-type layer, thus creating an important asymmetry of the P-N junction (Figure 5).

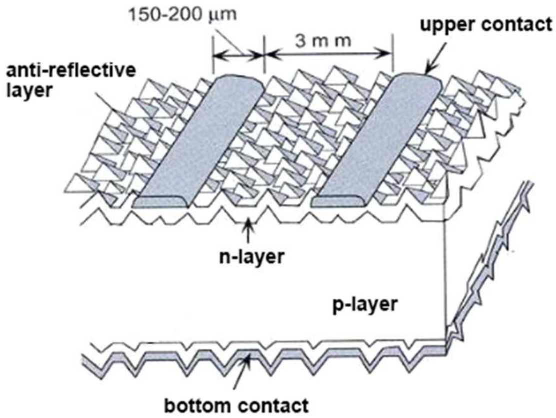

Figure 5. The structure of the first-generation cells [54].

The result of most research in the field of photovoltaics includes a functional prototype of a photovoltaic cell. To be able to compare photovoltaic cells with each other, it was necessary to introduce parameters that describe their quality. Most of these parameters are given by measurements of a specific product, whether they are DC or AC measurements. A very important indicator of cell functionality based on measured values is the volt-ampere characteristic (VACH). However, to enable comparison of these results on a global scale, standard test conditions have been introduced that define parameters with a great influence on the resulting values that describe the quality of the photovoltaic cell [55,56].

Standard test conditions:

- Lighting intensity 1000 W/m^2,

- Radiation spectrum AM 1.5,
- Temperature 25 °C.

To achieve standard test conditions, especially for the required spectrum of radiation as well as its intensity, a solar simulator can be used. With the help of several optical elements and systems, this device is able to imitate the required solar spectrum even with the prescribed intensity [56].

Photovoltaic cells are designed for a number of applications, be it energy or electronics, and their purpose remains the same, namely the generation of electricity. In the field of electronics, they find application mainly in devices that require a kind of energy independence, which can make a significant impact on the photovoltaic market. In this paper, the application in the energy industry is considered, where we require larger energy capacities from photovoltaics. In both cases, however, the efficiency of the energy conversion of solar radiation into electricity and the price of the photovoltaic cell are key. Research has dealt with the optimization of these important parameters for several decades [57,58].

2.3. Positioning of Photovoltaic Panels

Currently, positioning devices for photovoltaics are available in several designs and the main division is in the number of axes around which the photovoltaic panel, or field, can be rotated. Based on this number, we know one-axis and two-axis positioning devices. One-axis configuration assumes that one axis is fixed, and the other axis is positioned during the day. In the two-axis configuration, both axes are positioned, while their positioning direction consists of rotation around the vertical axis and a change in tilt with respect to the horizontal plane or positioning around the east–west axis and the north–south axis. Optimal pointing based on the position of the Sun is possible after sensing optical parameters or based on a model of the position of the Sun [58,59]. The complex positioning system proposed in this work considers the two-axis configuration and is based on model control; therefore, it must calculate the position of the Sun.

The position of the Sun relative to the observer on Earth is given by the Earth's orbit around the Sun, the rotation of the globe around its own axis and the position of the observer on Earth (Figure 6). However, the corresponding value is variable over time and the exact position can be calculated for a specific day and time. There are several calculation models, differing in their accuracy and calculation complexity. For our needs of positioning silicon-based photovoltaic cells, even less accurate and simpler calculation models are sufficient. The lower accuracy of the used model has practically zero impact when used in practice. The differences are minimal and are almost not reflected in the angular dependence of the generated power. The position of the Sun relative to the observer is expressed based on the following two angles: the azimuth and elevation angle. However, to calculate them, it is necessary to know other values explained below.

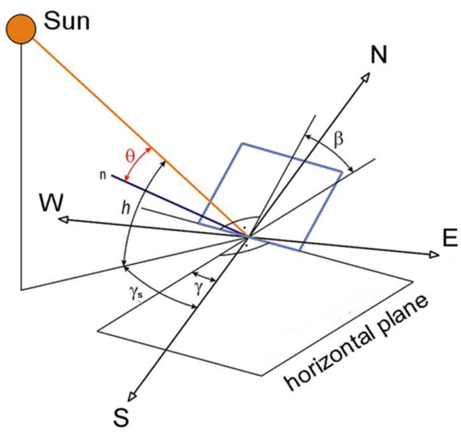

Figure 6. Geometric movement of the Sun relative to the receiving surface characteristics [46].

The angle of declination δ is the basis of practically every calculation for the position of the Sun. It expresses the angle between the connecting line of the centres of the Earth and the Sun relative to the plane created by the Earth's equator. It ranges from −23.45° to 23.45°. Only the day of the year is needed for the calculation, which can be observed in the following equation [60–62].

$$\delta = 23.45\sin\left(\frac{360}{365}(d-81)\right), \tag{12}$$

in which: d—day of the year.

The hour angle ω expresses the angle between the parallel solar radiation and the straight line given by the centre of the Earth and the position of the observer. It is positive in the morning hours, equals zero at lunchtime and gradually decreases with time. Since we need this value that is dependent on local time, its calculation must be divided into several steps and adjusted to the appropriate form. To calculate the local time, it is necessary to know the time zone ΔG_{TM} and the longitude D. The first step is the calculation of the time Equation (13) from which we obtain the EoT parameter. This is followed by the calculation of the time correction factor (14) TC and local solar time (15) LST, on the basis of which it is possible to determine the hour angle ω (16) [60–63].

$$EoT = 9.87\sin(2B) - 7.53\sin(B) - 1.5\sin(B), B = \frac{360}{365}(d-81), \tag{13}$$

$$TC = 4(D - 15\Delta G_{TM}) + EoT, \tag{14}$$

$$LST = LT + \frac{TC}{60}, \tag{15}$$

$$\omega = 15(LST - 12), \tag{16}$$

in which: D—longitude [°]; ΔG_{TM}—time zone; LT—investigated local time.

The elevation angle α expresses the angle between the plane of the observer and the straight line formed by the observer and the Sun, thus expressing how high the Sun is on the horizon (17). It can be determined by knowing the declination angle δ, the hour angle ω and the latitude ϕ [58–61].

$$\alpha = \cos^{-1}(\sin(\Phi)\sin(\delta) - \cos(\delta)\cos(\omega)\cos(\Phi)), \tag{17}$$

Azimuth A_Z is an angle that expresses the compass position of the Sun with respect to the observer, while it is calculated from the north pole in a clockwise direction, i.e., at solar noon $A_Z = 180°$. Another representation is that at solar noon, $A_Z = 0°$ and towards the east, it acquires negative values. Azimuth can be expressed based on the above angles (18) [60–63].

$$A_Z = \cos^{-1}\left(\frac{\sin(\delta)\cos(\Phi) - \cos(\delta)\sin(\Phi)\cos(\omega)}{\cos(\alpha)}\right), \tag{18}$$

Based on given relationships, we can determine the position of the Sun relative to the observer for a specific position on Earth and a specific time using the angle of elevation and azimuth. For this reason, we do not need to have images of the position of the Sun available, and when rotating the right photovoltaic panel, we will only need the current rotation in both planes.

3. Design and Implementation of the Complex Mechatronic Positioning System

In this section, we describe the design and implementation of the mechatronic positioning device and the implementation of the control system. Finally, we present a software application for energy system visualization. The design of a positioning system aims at enhancing efficiency of obtaining energy from a renewable source. In our case, as has already been mentioned, it is a positioning mechatronic system on two axes that ensures the optimal tilting of the photovoltaic panel perpendicular to the incident sunlight. Photovoltaic panels, for which this positioning system is intended, are the most widespread on the market and their technology is the most researched, so they are panels based on crystalline silicon. As mentioned in the analysis of the energy system, the angle under which the solar radiation falls on the plane created by the surface of the panel has a fundamental influence on the amount of incident energy and its subsequent transformation into electrical energy. Thus, the positioning device increases profit in generated power during the day in comparison with a fixed panel, but it consumes a certain amount of the obtained energy for positioning. The amount of energy input to the positioning must be minimized; therefore, the design of the mechanical as well as the drive system is very important.

3.1. Hardware Design and Implementation of Mechatronic Positioning Device

Hardware design basically consists of the following three main parts: the photovoltaic panel, console, and drive unit. The design for the optimal photovoltaic panel is also determined by the geographical location in which the given positioning system will be installed. For different geographical locations, optimal construction designs and their control can be different. In this work, we consider the geographical location of Bratislava; therefore, the design of the mechatronic system will be primarily focused on the corresponding latitude [63]. In this subsection, the requirements for the design of a mechatronic positioning device for photovoltaic panels for roof applications are defined. The following requirements for the positioning system are subsequently analyzed in order to fulfil them:

1. Movement variability, which enables us to orient the photovoltaic panel perpendicularly to the direction of the Sun's rays for each position of the Sun for a given geographic location, while the maximum permissible deviation is 15° from the perpendicular incidence of the rays on the panel at the extreme of the Sun's positions.
2. The positioning accuracy of the normal vector of the photovoltaic panel to the desired point determined by the azimuth and elevation angle relative to the positioning device with an accuracy of $\pm 2.5°$. Positioning accuracy must be ensured over the full range of motion of the device.
3. The robustness of sensing the angle of rotation of individual tilting axes of the photovoltaic panel.
4. The design of the structure and mechanical parts of the mechanism must meet all the attributes for the minimum energy requirements for the propulsion system.
5. Ensure a fixed position over the full range of the positioning, which will prevent rotation around both axes caused by external influences.
6. The structure must be installable on the flat roof of the building, while it must be able to withstand weather effects of wind, rain, temperature and sunlight. Even under these influences, the positioning system must achieve a sufficient service life as well as minimal maintenance during the operation of the device.
7. A variable console that allows fixing available panels on the market, as the dimensions of the panels are not standardized and may differ slightly from different manufacturers. The bracket must be able to carry the load due to the influence of the panel as well as other influences. The permissible load capacity of the installed panel is at least 25 kg and the necessity of the possibility of height variability, which allows us to find an equilibrium position for different panels.
8. The design shall allow multiple positioning devices to be connected to one common drive system. The design shall allow the connection of individual positioning devices for both tilting axes.
9. A complex mechatronic positioning system of photovoltaic cells should have as small weight as possible, under all prerequisites for mechanical resistance and durability. The weight is important because of the installations on the roof of the building.
10. The system must be manufacturable on the basis of available materials and technologies in common practice, with the lowest possible production price. The system

must be capable of being assembled and allow for the possible replacement of any component without significant intervention.

The range of mobility of the mechatronic positioning system for the purpose of increasing energy efficiency, and therefore increasing the generated power of photovoltaic cells, depends on the position of the Sun. The position of the Sun changes during the day and the trajectory of the Sun across the sky is dependent on the latitude of the given energy system.

We can express the position of the Sun using two angles, namely the elevation angle and the azimuth angle relative to the system (for more details, see Section 2.3), that is, to the geographic location of the system installation [33,63]. For applications of this system, we start from the geographical location of Bratislava, where the latitude is S 48°1′ and longitude is E 17°11′ [63]. The annual course of the elevation angle at solar noon in Bratislava is shown in Figure 7. It is obvious that azimuth changes during the light phase of the day depending on the current season, as it is shown in Figure 8.

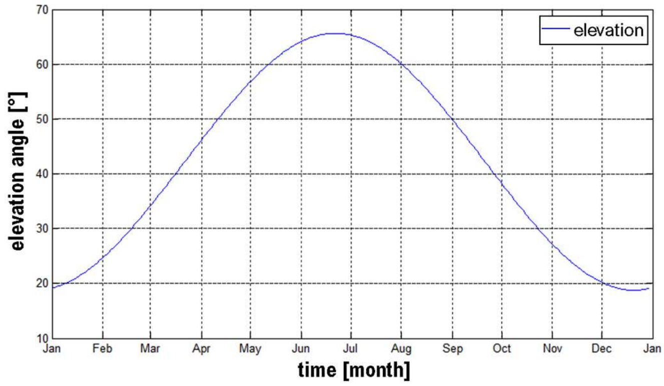

Figure 7. The annual course of the elevation angle at solar noon.

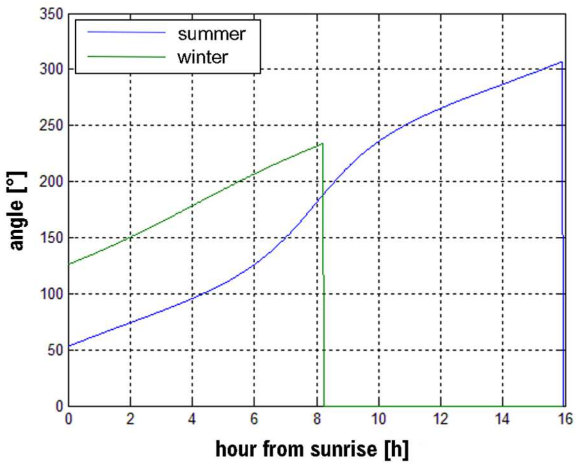

Figure 8. Azimuth curves for the solstices in the light phase of the day.

The variability of the console is based on requirement 7 and is supposed to provide several essential functions. In addition to the need for a sufficient load-bearing capacity, it must also fulfil other essential parameters related to the energy requirement of positioning as well as the universality of the mechatronic system for positioning photovoltaic cells, which can be of different sizes from different manufacturers. Note that the knowledge of these parameters at the stage of design preparation is essential and it is very important to analyze them before the design process.

Structural design takes place in the CATIA program environment [64]. This development tool enables modelling of 3-D objects in a virtual reality environment. It contains many modules that provide various functions or analyses. For the needs of our work, the PART DESIGN module, which enables 3-D modelling of individual bodies, is perfectly suited and the ASSEMBLY DESIGN module allows the individual modelled bodies to be interconnected into complex mechanical systems. Both modules fall under the category called MECHANICAL DESIGN.

The modelled mechanical systems using the mentioned modules are composed of several bodies that are fixed to each other by bindings. Bindings can be different, but because it is a mechanical system, it also contains bindings that introduce a certain number of degrees of freedom between individual bodies into the system. It must also be noted that the dynamics of movements, and thus also the action of forces, will be solved through the MSC ADAMS program, which is much more suitable for these tasks.

At the beginning of the design and modelling process is the photovoltaic panel, from which the subsequent design of the structural solution is based. The photovoltaic panel, i.e., its dimensions and weight, represents the input and an uninfluenceable parameter of the design. It is, therefore, obvious that the design of other components of the mechatronic positioning device will be based on those values. Its basic parameters are shown in Figure 9.

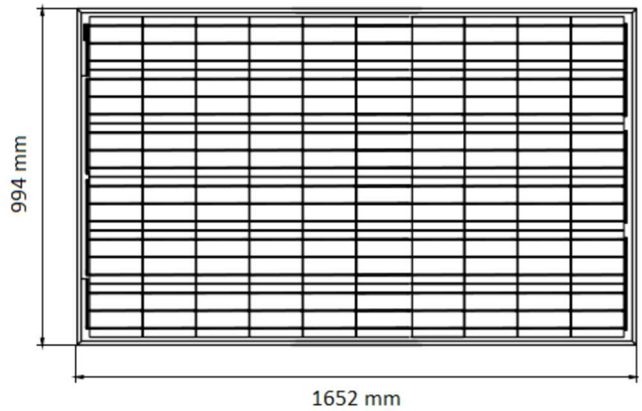

Figure 9. Photovoltaic panel drawing.

Basic parameters of the photovoltaic panel:

- ○ Technology: polycrystalline;
- ○ Nominal power: 250 Wp;
- ○ Efficiency: 15.2%;
- ○ Dimensions: 1652 × 994 × 40 (mm)
- ○ Weight: 20 kg (without frame);
- ○ Composition: frame, glass, module, EVA and back cover;
- ○ Glass thickness: 3.2 mm.

A view of the frame model can be observed in Figure 10a and a cross-section of the internal structure with single layers of the panel is shown in Figure 10b. The final model of the photovoltaic panel is shown in Figure 11a with the used materials such as aluminium, glass and the photovoltaic module.

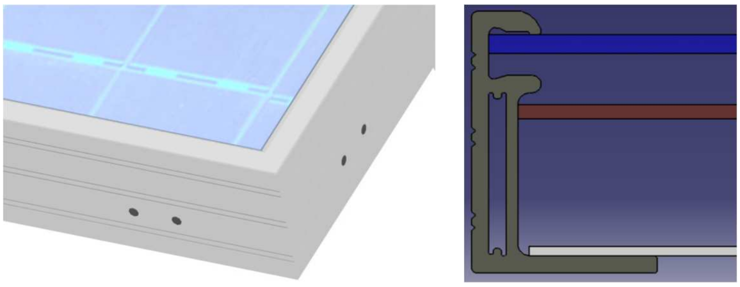

(**a**) (**b**)

Figure 10. Frame detail (**a**); cut through the panel (**b**).

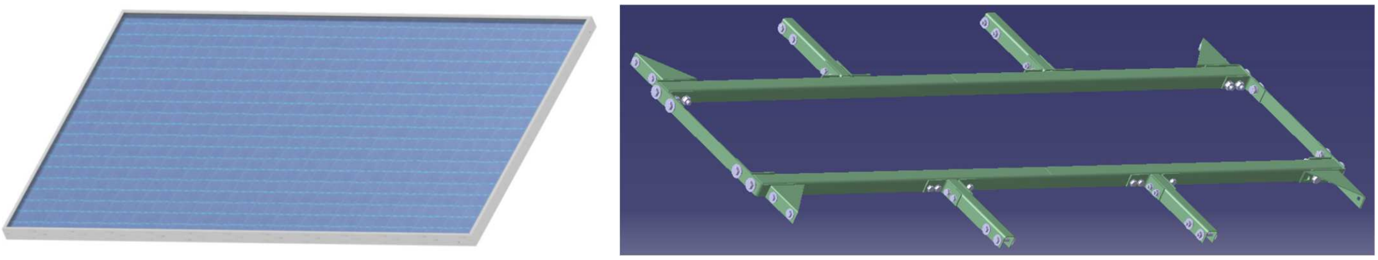

(a) (b)

Figure 11. Photovoltaic panel model (**a**); bracket without fasteners (**b**).

The design of the console is based on the established requirements and parameters of the photovoltaic panel. The main conditions for the proposal are sufficient load capacity, the possibility of the secure attachment of the panel, the mentioned variability of fastening elements and the possibility of height adjustment in relation to other components of the positioning system. Great emphasis is also placed on assembly ability, as well as the use of real and available structural elements. The base of the console construction is shown in Figure 11b.

The entire system consists of the base of the positioning system, drive, and shaft position sensor. In Figure 12, we can observe a two-axis complex positioning system of photovoltaic cells. Based on positioning using individual actuators and the collision detection function, the extreme positions of the system were found. With the help of these extreme positions, it is possible to determine the range of system mobility expressed in the rotation angles of the individual shafts of the rotation axes (Table 2). These angles do not directly express the direction of the normal vector of the panel.

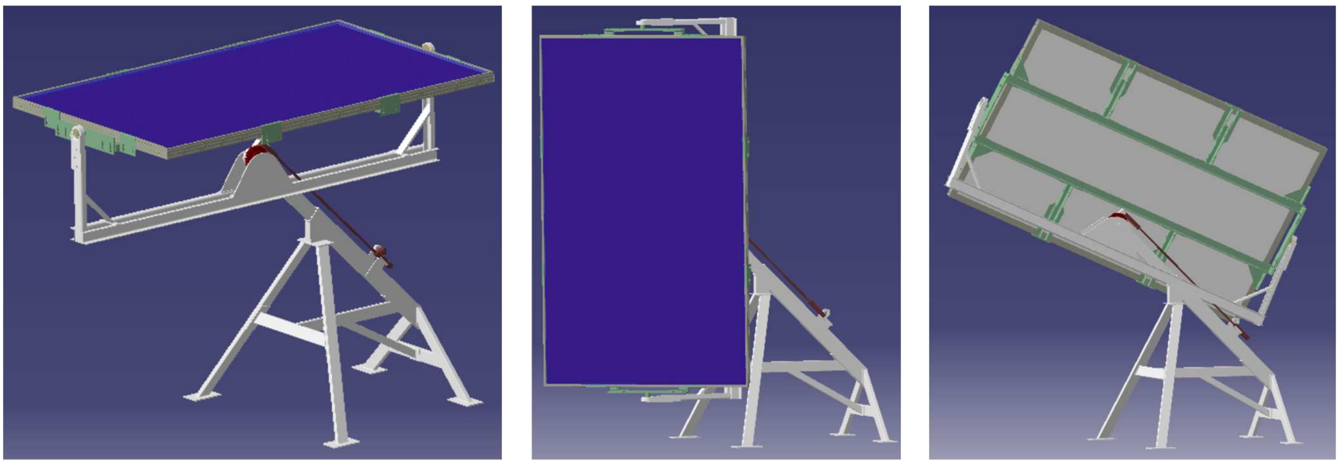

(a) (b) (c)

Figure 12. Complex positioning system (**a**); extreme positions of the mechatronic positioning system (**b**,**c**).

Table 2. The mobility range of the designed photovoltaic panel positioning system.

	North–South Axis	East–West Axis
From	−20°	82°
To	−75°	75°

The aim is to design a system that ensures optimal conditions for maximizing the efficiency of the energy system. The evaluation of the energy demand of positioning can be determined if the electrical parameters of the motor with which the given photovoltaic system is positioned are known. In order to correctly choose the drives, i.e., the positioning motors, it is necessary to know the static and dynamic moments in individual positions and movements.

We use a stepper motor as an actuator for the positioning of the photovoltaic panel. To specify the parameters of a stepper motor, a mechanical analysis of the positioning system was performed. Thus, the maximum torques arising during the positioning of individual axes were obtained. The analysis was carried out in the positions that correspond to the maximum torques; therefore, it has a sufficient informative value for the stepper motor specification.

The choice of the stepper motors for each axis was, therefore, based on the size of the step, sufficient torque as well as the minimal energy requirements. The choice of the gear ratio was also very important, because a larger ratio will ensure a greater torque, but at the expense of the number of steps the drive must perform. However, with the number of steps, the time of its operation and thus its energy consumption also increases; therefore, it is important to find the right compromise for the choice of this parameter. For the needs of using a stepper motor, a mechanical analysis of the positioning system was performed, based on which the maximum torques that arise during the positioning of individual axes were given. The analysis was performed in the positions of the largest moments (Table 3); therefore, it has a sufficient informative value for the dimensioning of the stepper motor.

Table 3. Results of the mechanical analysis of the positioning system.

Results of Static Analysis of the Positioning System	
Maximum static moment of the VZ axis	0.6 Nmm
Maximum static moment of the SJ axis	28.5 Nmm
Results of the Dynamic Analysis of the Positioning System	
Maximum dynamic moment of the VZ axis	0.52 Nmm
Maximum dynamic moment of the SJ axis	0.97 Nmm

The parameters of the selected stepper motor that correspond to all the requirements are summarized in Table 4.

Table 4. Parameters of the selected stepper motor.

Parameter	**Value**
Nominal torque	1.89 Nm
Nominal voltage	3.2 V
Nominal current	2.8 A
Number of windings	4
Winding resistance	1.13 Ω
Inductance	3.6 mH
Rotor inertia	480 g·cm^2
Holding torque	0.068 Nm

3.2. Simulation Software of Mechatronic Positioning Device

After designing the structure solution, we know the working range of mobility, based on which we can calculate the energy gain compared to fixed photovoltaic panels. The proposed complex mechatronic positioning system can be verified at this stage thanks to the capabilities of advanced computer technology and software equipment. In the MSC ADAMS program environment [65], the designed model of the positioning device can be controlled using co-simulation with the MATLAB computing environment [66]. The cooperation of these two programs is based on exporting the model from MSC ADAMS to MATLAB. This export is based on the definitions that determine which parameters should be available for the output model, whether they are input or output variables. However, for the needs of functionality verification, it is important to verify the functionality of the stepper motor for individual tilt axes, for the moments arising in the system, as well as the control frequency of the stepper motor. Therefore, the simulation scheme (Figure 13) contains blocks that describe the behavior of individual components of a complex mechatronic system. The basis is a block that represents the designed model of the photovoltaic panel (orange block in Figure 13). The inputs to this model are the tilting moments on individual positioning axes. The outputs are the moments that were analyzed and the tilt position of the individual axes.

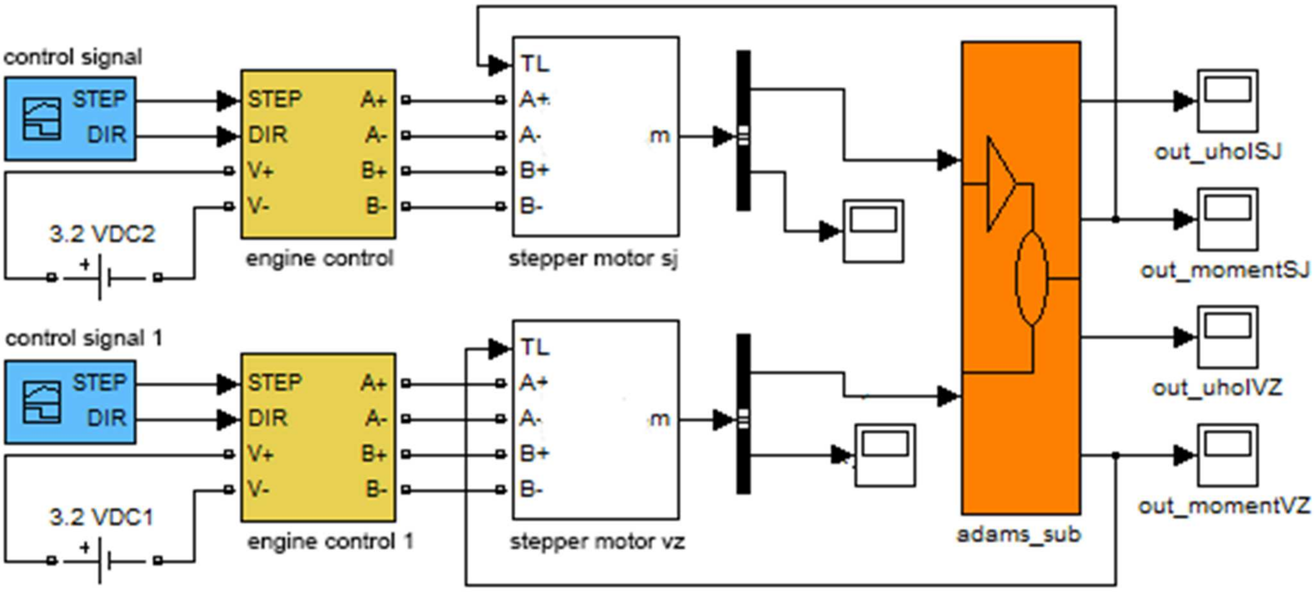

Figure 13. Simulation scheme of a complex positioning system.

Other blocks in the simulation scheme are the stepper motors (white blocks) that position the panel in individual axes. The outputs of these blocks are the torques generated by the stepper motors based on the input signals from the engine control blocks (yellow blocks). The input to the stepper motor block is the power supply of the individual windings, as well as the load torque. The control of the stepper motor (yellow blocks) ensures the switching of the voltages on the individual windings and ensures the change in the shaft position through pulse-width modulation. The input signal to the engine control block is a control signal that determines the operation as well as its direction. The second input is the supply voltage, which is transferred to the motor windings. The control frequency is 10 Hz and the block that describes the stepper motor has the parameters corresponding to a stepper motor designed at the end of Section 3.1.

The task of this simulation is to verify the correct operation of the motors under the influence of the load arising during the positioning of the individual axes of the system. If the stepper motor was loaded with a large torque, the step could be lost; thus, the positioning of the system could malfunction. In simulation results, we can monitor this phenomenon, whether the motor step is not lost due to the load.

The resulting responses (Figure 14) show the electromagnetic moment of the stepper Wmotor, i.e., the moment by which we position the device and especially the position of the motor shaft, and oscillations indicate the mentioned malfunction. The response is shown at a higher load and the results show the moment generated by the stepper motor, as well as a stable step change in a given interval with a change in size corresponding to one step, thus verifying the functionality of the photovoltaic panel positioning system designed in this way.

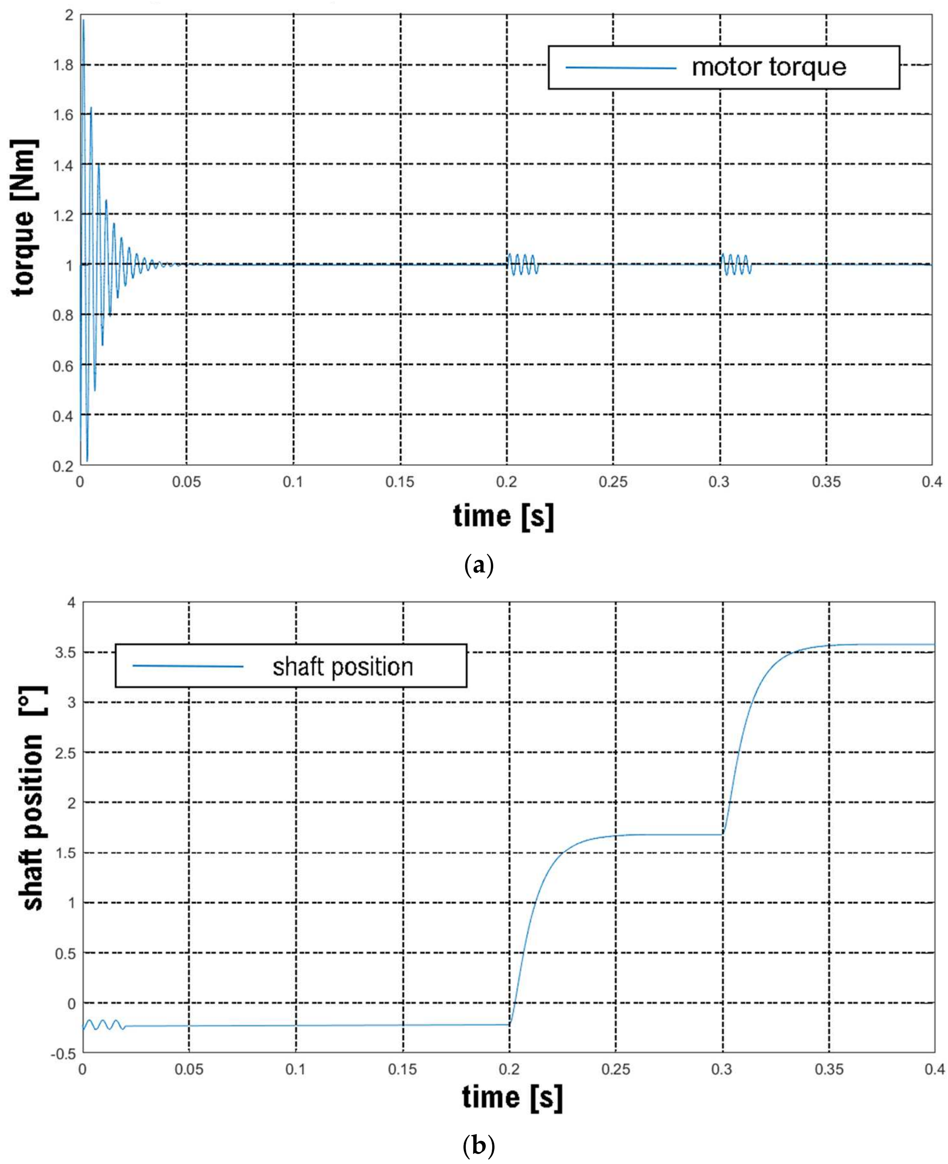

Figure 14. Simulation responses for motor torque (**a**); shaft position (**b**).

It can be observed in Figure 14 that the co-simulation of the position control for the east–west axis of the photovoltaic system in the MATLAB Simulink environment took place as expected, i.e., with each request to change the position from the control signal block (see Figure 13). This change will be reflected by vibrations for the response of the stepper motor torque and the following correct change in position of the entire photovoltaic panel.

The x-axis shows the time in seconds, and the y-axis shows the motor torque in Nm in the upper part of the picture, and the turning angle in ° in the lower part.

3.3. Program Implementation of the PLC Control System

A control element that ensures the operation of the system must also be part of the complex mechatronic system for positioning photovoltaic cells. Its function primarily consists of the control of stepper motors in order to efficiently position the photovoltaic cells in relation to the energy source, i.e., towards the Sun. Optimal positioning ensures optimal efficiency of obtaining electrical energy from the photovoltaic energy system. In addition to the control of the stepper motors, the controller must also calculate the optimal pointing based on the position model of the Sun, since this is a design without any optical sensing of the Sun's position. The positioning system must be able to determine when it is optimal to position the photovoltaic panel, that is, the moment when the deviation of the normal vector of the panel and the position of the Sun is greater than optimal. However, the optimality as well as the possibility of positioning the photovoltaic panel towards the Sun are also determined by weather conditions, which the control system must take into account.

The program solution can only be verified in practice by running the program on a real PLC control system. In such cases, another part of the STEP7 software [67] is used to verify the functionality of the program, which is the PLCSIMULATOR, that enables the tuning of the given program. The PLCSIMULATOR is, therefore, an essential part of program implementation in the case when a real PLC is not available.

In practice, the use of PLC devices would depend on the scale of the photovoltaic panel system; in the case of one photovoltaic panel, a Siemens Logo PLC device would be sufficient, the current price of which is approximately EUR 150. In the case of several devices with up to 10 photovoltaic panels, a PLC device S7-1200 or equivalent would be needed, the price of which is about EUR 500. In addition, in the case of several devices over 10 photovoltaic panels, it would be necessary to use a PLC device S7-1500 or equivalent with input/output modules, where the price would start from EUR 2000 and more, depending on the number of panels.

The control algorithm, as well as the entire positioning system, are designed to minimize their own consumption. The control program solution has a fundamental influence on the running of the drives, while it is necessary to avoid unnecessary steps or that the drives run due to the incorrect positioning of the system. This is the priority of the design of the entire control algorithm, which must be ensured if the energy input to the positioning system of the photovoltaic panels is to be minimized.

The software solution itself is designed to minimize the consumption of the control system, that is, it performs only the immediate necessary steps. For the positioning of the photovoltaic panels, a frequent change is not necessary; therefore, it is not necessary to perform all the calculations in each program cycle. The duration of the execution of one program cycle is determined by the length and complexity of the program, but it varies in units of a maximum of tens of ms. Thus, it is sufficient that the deviation of the Sun's position is compared to the normal vector of the photovoltaic panel, which is preceded by the calculation of the Sun's position, as well as the direction of the vector, only once every minute using a cyclic PLC interrupt. Therefore, as part of the execution of each program cycle, only an evaluation of the possible fault conditions or operator interventions is realized.

The calculation of the position of the Sun is composed of several functions that ensure the calculation of all necessary parameters. After determining the position of the Sun, the direction of the normal vector of the photovoltaic panel is calculated. The calculation of the normal vector is given by the structural solution of the positioning system and is based on the value obtained by the position sensors on the individual positioning axes. After calculating these two values, the control system can evaluate the deviation and, based on the determined value, declare whether it is necessary to change the current position or not. When requesting a change in location, a subsequent evaluation of weather effects is necessary, which, if favourable, is followed by a positioning algorithm that ensures the optimal positioning of the photovoltaic panel with the aim of maximizing energy gain. The positioning algorithm determines the optimal direction of the normal vector of the panel; based on this direction, it determines the required rotation of the individual positioning axes of the system. After determining the desired value as well as the direction of the desired change, it starts the individual drives until they acquire the desired value. The control algorithm is clearly summarized in the flowchart of the positioning software solution in Figure 15.

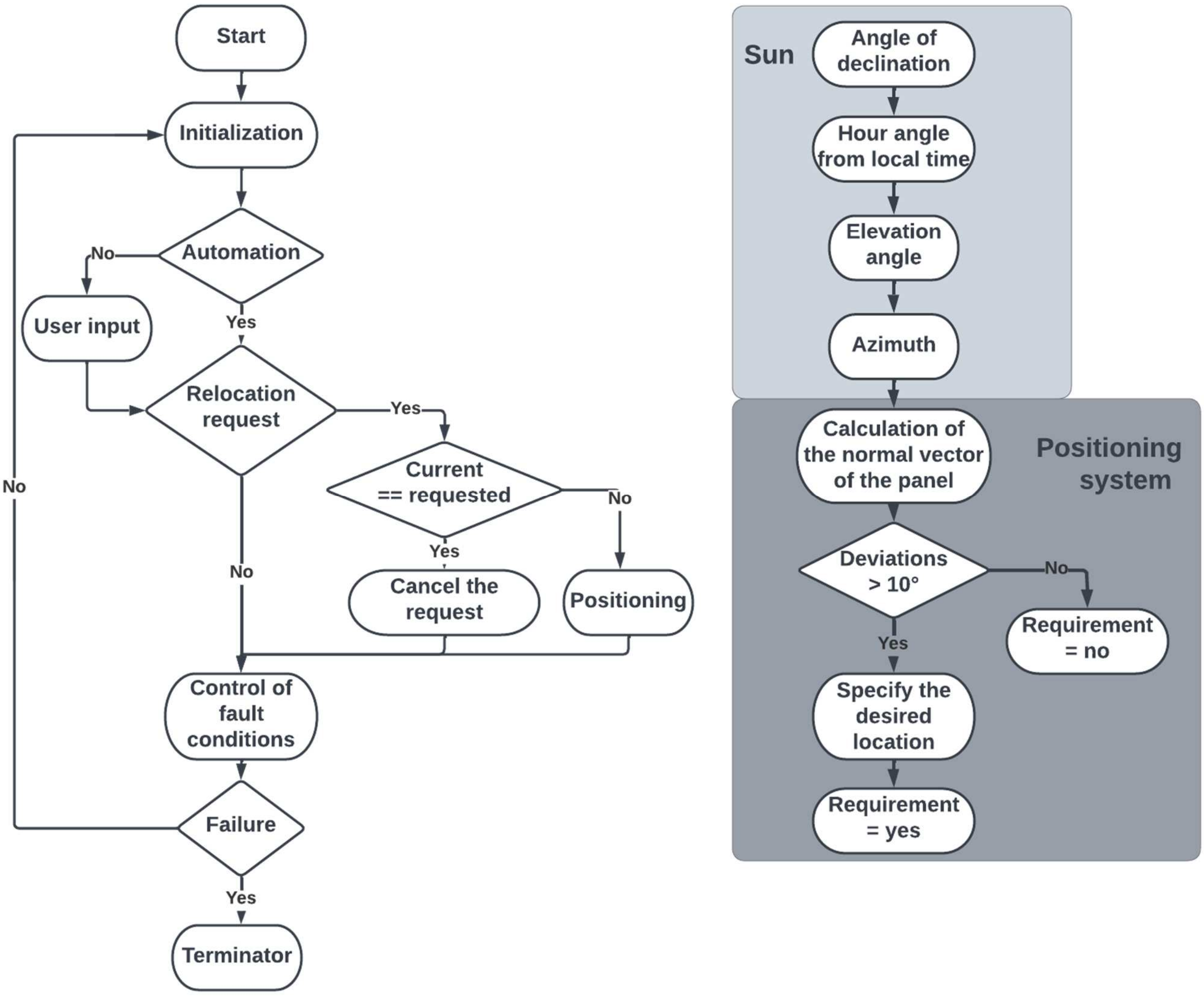

Figure 15. Development diagram of the control algorithm.

The development of the photovoltaic panel positioning control system was based on the following requirements, and we can conclude that the proposed algorithm fulfilled them.

(1) Sufficiently accurate calculation of the position of the Sun with respect to the positioning system of photovoltaic panels.
(2) Identification of unsuitable conditions for panel positioning in terms of energy demand in relation to gain, i.e., in cloudy periods when direct sunlight does not pass through. It is considered essential to use a solar radiation intensity sensor for the real system. In case the measured value is below the specified minimum, the panel will be moved into the default position.
(3) Weather effects in the form of high wind speed must be considered, which is important especially for safety reasons. In this condition, it is necessary to minimize the stress of the structure and to prevent an increased energy demand, caused by the positioning of the panel under strong wind. In case of wind speed above the critical value, the control system must ensure the position in which the system is least affected by this factor.
(4) The positioning algorithm must ensure rotation to the optimum position. The optimum position is given by the current position of the Sun, and the control system must be able to ensure that the normal vector of the panel is positioned to this point. The position must be determined accurately, and the positioning must be performed

with a minimum number of steps, without searching for the optimal position by positioning the panel.

(5) The control system must be robust under various unfavourable conditions, for example in the event of a power failure, where the system must remain fixed, and after restarting, it must be able to identify its position and optimize it by a potential correction with a minimum number of steps.

(6) The control system must be able to identify potential malfunctions and take adequate measures to correct them, and if this is not possible, ensure that the operator is informed of the malfunction.

(7) Positioning to any direction of the normal vector of the positioning device panel, specified by the operator.

3.4. Creation of a Software Application for Visualization of the Photovoltaic System

It is necessary to create a program environment that enables a human–machine and machine–human interface with the given controlled process of positioning photovoltaic panels. For our photovoltaic energy process equipped with a positioning photovoltaic panel system, it is important to have an overview of the positioning equipment as well as the position of the Sun to verify the functionality of the positioning process. The visualization application should give the operator an overview of the theoretical value of the incident power, but especially of the electrical power generated by the power system based on conversion from solar radiation. The visualization must be implemented in conjunction with the PLC control system of the positioning device. The WINCC FLEXIBLE program environment enables the creation of HMI interfaces for these control systems [68]. The main parts of the proposed visualization system are the screen header, main screen, overview of alarms, graphic evaluation, and manual operation control panel. These parts are described in detail in the subsections below.

The design of the visualization environment is based on the requirements and needs of the given positioning process. Therefore, the structure of the visualization environment is directed to provide a clear view of the process with all the important parameters displayed. These are divided into sections according to their affiliation, allowing the operator quick access to the necessary data as well as the possibility to intervene in positioning the photovoltaic panels. This is performed in the form of an arbitrary intervention and can trigger any state of the positioning device. The structure of the visualization environment enables the operator to have an overview of the progress of the process variables using a clear display on the screen with a graphical design. Another important screen of the visualization environment is the list of alarms, which allows an overview of the operation of the device from the point of view of faults and warning messages for the selected period.

When designing a visualization environment, the availability of key information and the ability to actively intervene at any time, i.e., on every screen, is important. Therefore, the operator must be able to select the manual or automatic mode of operation of the positioning system or have the possibility to switch between the different screens that offer the visualization of the positioning of the photovoltaic panels.

3.4.1. Screen Header

The header of the visualization screen consists of two parts, the part equipped with navigation and control buttons and the part that displays the current values that correspond to the controlled process. The part containing the buttons is displayed in each screen. The representation of the header of the visualization environment is shown in Figure 16, where both mentioned parts of the header are displayed.

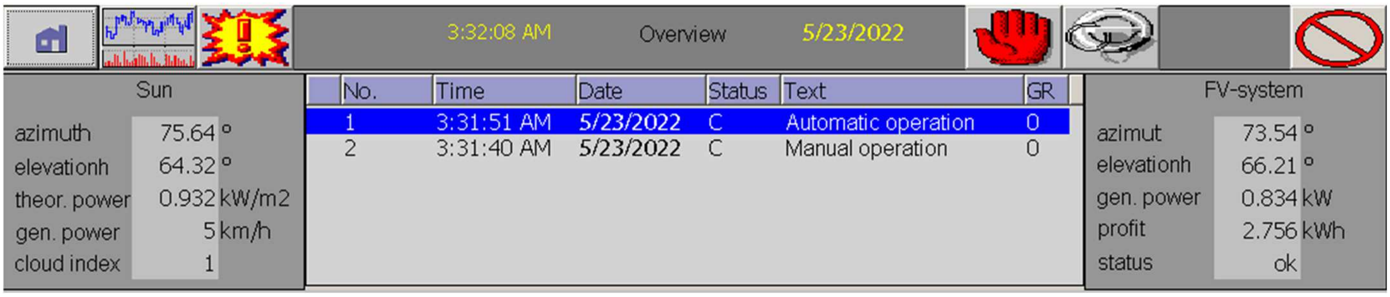

Figure 16. Header of the visualization environment.

The navigation part of the header of the visualization environment is located at the very top of the header, and therefore also at the top of all visualization screens. Its implementation is solved using a template, which ensures its application to all screens. The navigation section contains the following elements in order from the left to the right:

- Main screen panel button,
- Graphical evaluation panel button,
- Alarm overview panel button,
- Middle part with current time data and the panel just opened,
- Button for activating manual operation,
- Button for activating automatic operation,
- Ending the visualization.

The overview part is located right below the navigation panel of the header of the visualization environment. This overview section offers a clear display of the most important information about the process, as well as active error reports. The overview section is divided into three segments, the left segment is an overview of information about the Sun, followed by an overview of active alarm and fault reports, and the last segment is dedicated to important information about the positioning system.

3.4.2. Main Screen

The main screen of the designed visualization environment offers an overview of all available information about the process. The screen consists of the mentioned header and other elements offering a clear display of the given values. The main part of the screen is again divided into several segments that display values related to and belonging to specific elements of the designed complex mechatronic system for positioning photovoltaic panels.

The main part of the screen of the visualization environment is made up of three sections that belong to individual parts of the screen. The structure of individual sections is clearly located in individual parts of the given screen. In the left part of the screen, there are sections of the generated power; in the central part, there is a section of the visual display of the positioning device together with the outputs of the measured values, through which it is possible to display the rotation angles around the individual axes. In the right part, there is a section dedicated to the meteorological station. The resulting design of the main screen is illustrated in Figure 17.

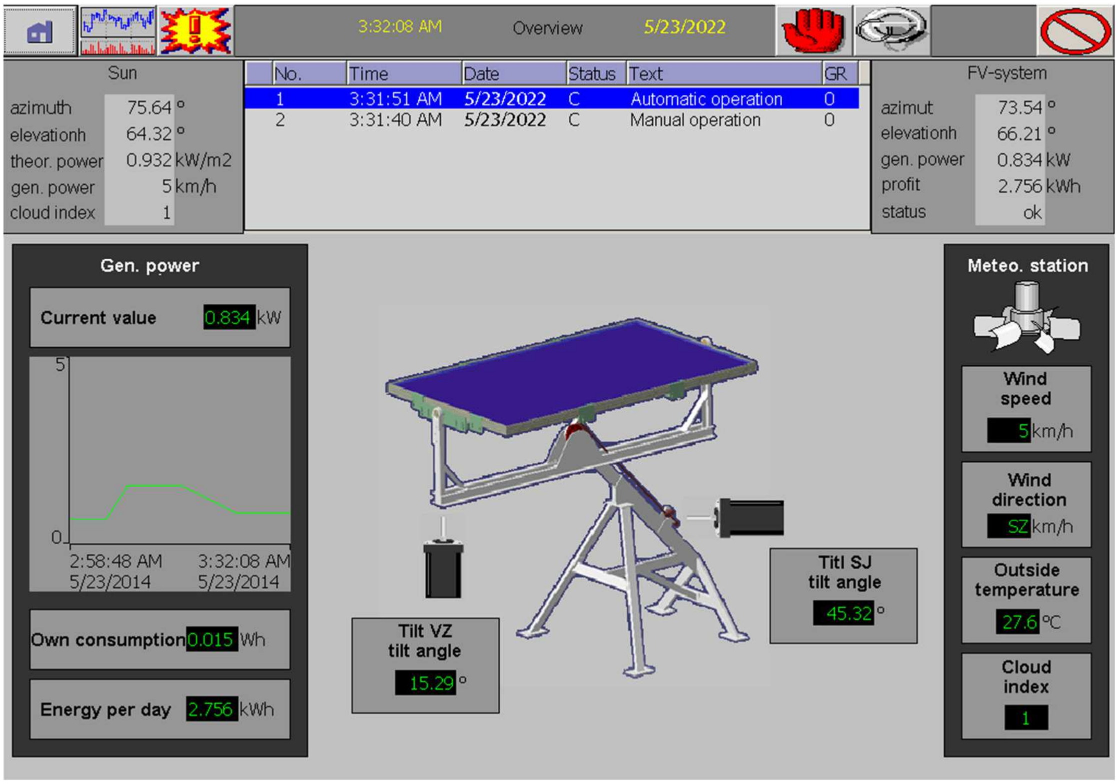

Figure 17. The main screen of the visualization environment.

3.4.3. Overview of Alarms

The operator of the complex mechatronic system for positioning photovoltaic panels must supervise the correct operation of the device. After evaluating any fault condition or warning message, the operator is informed about this fact in the form of a warning sign by writing a fault message in the corresponding light in the overview part of the screen. However, as stated above, only active fault or warning messages are displayed in this screen (Figure 18). After they have passed, the message from this window disappears; therefore, it is important to provide the operator with a retrospective evaluation of faults.

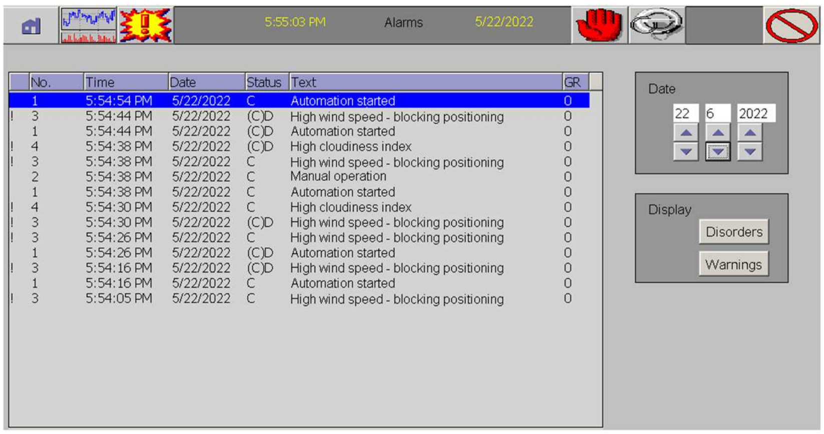

Figure 18. Alarm messages screen.

For the retroactive evaluation of fault conditions as well as warning messages, it is necessary to create a screen within the visualization environment that provides an overview of fault messages and their history. Within this screen, the operator must also have the option to display these fault and warning messages for a specified day in the past. The size of the volume of data that can be retrospectively evaluated is given by the database system, which, however, is not the included in this work.

3.4.4. Graphic Evaluation

The design of the visualization environment allows the operator, in addition to observing the current values, the possibility to observe the behavior of the determined variables for the selected period. The screen dedicated to the graphical evaluation of the process variables allows the operator to observe the selected variables using the progress in the graph. The operator has the option of looking back in time through the mentioned graph. However, to ensure the desired selection, the screen must also contain control elements that enable the operator to perform the given action (Figure 19).

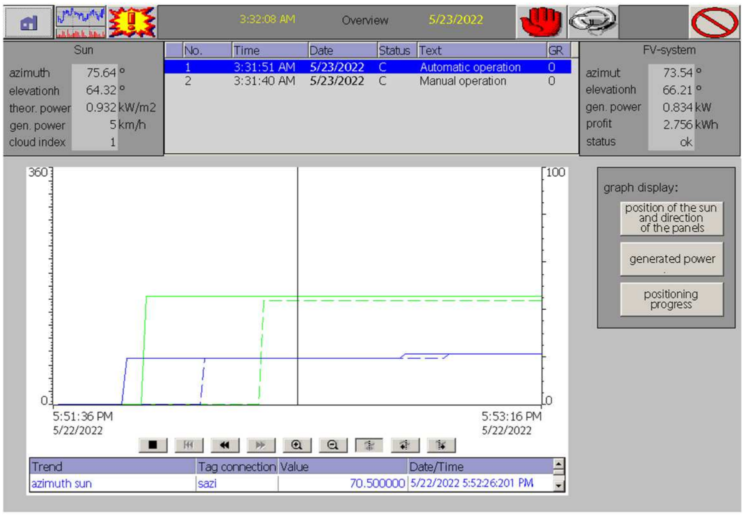

Figure 19. Graphical evaluation screen of process variables.

3.4.5. Manual Operation Control Panel

The device operator has the possibility to influence the positioning device based on a specific request. In practice, this means that the operator has the option to choose the manual operating mode of the control system, during which the automatic positioning of the photovoltaic panels to the optimal direction is not carried out. During this selected mode of operation, the operator has the possibility to perform any positioning of the panel (Figure 20). The need for this option is because maintenance and service operations may occur during operation, when the operator must be able to ensure the positioning of the system in the selected position to perform these operations.

The proposed solution of the visualization environment enables manual operation to be invoked using the header, which contains a button for activating the manual operation of the positioning control system. After pressing the button, manual operation is immediately selected, and the manual operation controller window is displayed. Starting manual control is possible from any screen. The user has the option to hide one of the four predefined positions, which can be achieved by pressing the corresponding button. These predefined positions make it easy for the operator to recall the most frequently used positions.

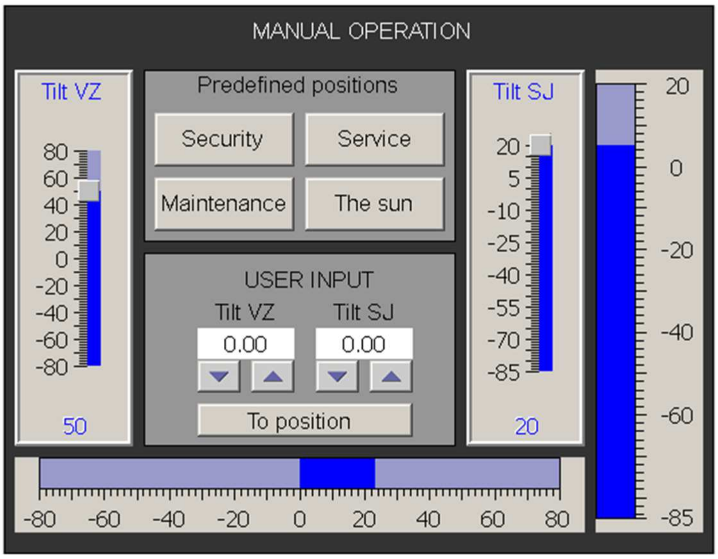

Figure 20. Manual operation controller.

4. Results

This section presents the results of the simulation experiments with the simulation model developed in the previous section and its evaluation. The evaluation process as well as the simulation calculation are performed in the MATLAB program environment, which assists with the calculations, further graphical evaluation of the positioning process and the evaluation of the energy balance. For the overall evaluation of the results of the complex mechatronic system for positioning photo-voltaic panels in energy applications, it was necessary to perform several partial analyses.

The first analysis included in the corresponding calculations is the analysis of the movement of the Sun during the year, while simultaneously evaluating the incident solar energy on the optimally oriented plane. The plane is optimally oriented when its normal vector points exactly to the Sun, the incident rays are perpendicular and there is maximum efficiency in converting solar energy into electrical energy. The value given in this analysis tells us the amount of incident energy per year in a given area (Figure 21). The calculations start from the geographical position and a specific time, which determines the position of the Sun. Based on this position, it is possible to determine the atmospheric effect coefficient for specific input parameters. The size of this atmospheric effect coefficient determines the amount of solar energy passing through the atmosphere without absorption to the Earth's surface (Figure 22). Its size has a fundamental influence on the solar energy falling on the optimally oriented plane on the surface of the Earth.

Another part of the analysis concerns the design of the positioning algorithm for the photovoltaic panel, which means that in the computing environment, the course of the positioning process is simulated throughout the year based on the trajectories of the Sun. Then, the amount of energy incident on such an inclined plane can be evaluated.

When simulating the positioning algorithm of a mechatronic system designed for power systems, it is necessary to also simultaneously evaluate the power consumption required for this positioning with the panel positioning. The energy expended in positioning the photovoltaic panel must be as small as possible if the energy gain is to be ensured compared to the fixed panels.

The evaluation of the achieved results is based on a simulation, which will ensure the recalculation of values throughout the year by minutes based on the position of the Sun, thus determining the light parts of the day. Calculations of incident energy as well as a positioning algorithm are subsequently applied to the data that determine the position of the Sun during the day. Simultaneously with the evaluation of these factors, the energy incident on the fixed-oriented panel is also evaluated, based on which we have to determine the energy gain.

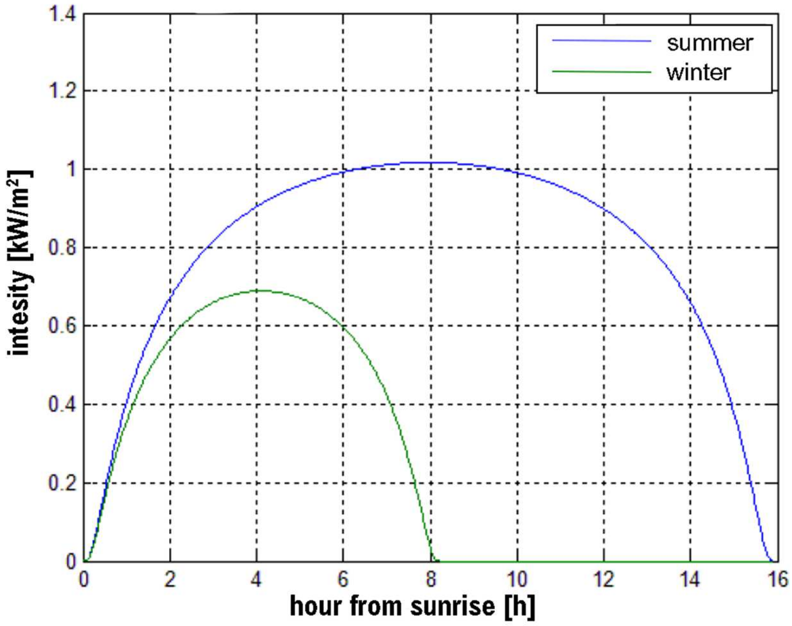

Figure 21. The daily course of solar radiation intensity during the days of the solstice.

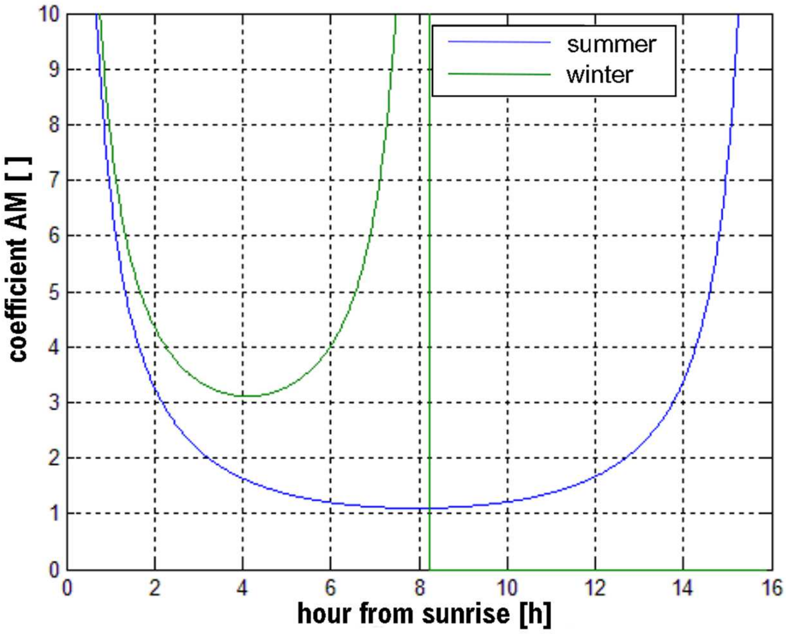

Figure 22. Daily course of the atmospheric effect coefficient during the days of the solstice.

When sunlight hits the inclined surface of the panel at a certain angle, reflection occurs, while the intensity of the incident radiation on the deviated plane is reduced by the corresponding values. The intensity of the radiation incident during the year on a panel positioned by the system or fixed can be calculated based on the above-mentioned influence. The effect of this decrease in intensity is given by the size of the deviation angles in individual directions that express the position of the Sun. The calculation used to evaluate the intensity incident on the I_P panel (19) is based on the intensity of the radiation incident on the optimally inclined plane and the relationship describing the angle difference (Figures 23 and 24).

$$I_P = I_G(\cos(h)\sin(\beta)\cos(\gamma - \gamma_s) + \sin(h)\cos(\beta)), \tag{19}$$

in which: I_G—intensity of radiation in a semiconductor $[\frac{kW}{m^2}]$; h—the elevation angle of the Sun [°]; β—panel tilt [θ]; γ—azimuth of the panel [θ]; γ_s—azimuth of the Sun [θ].

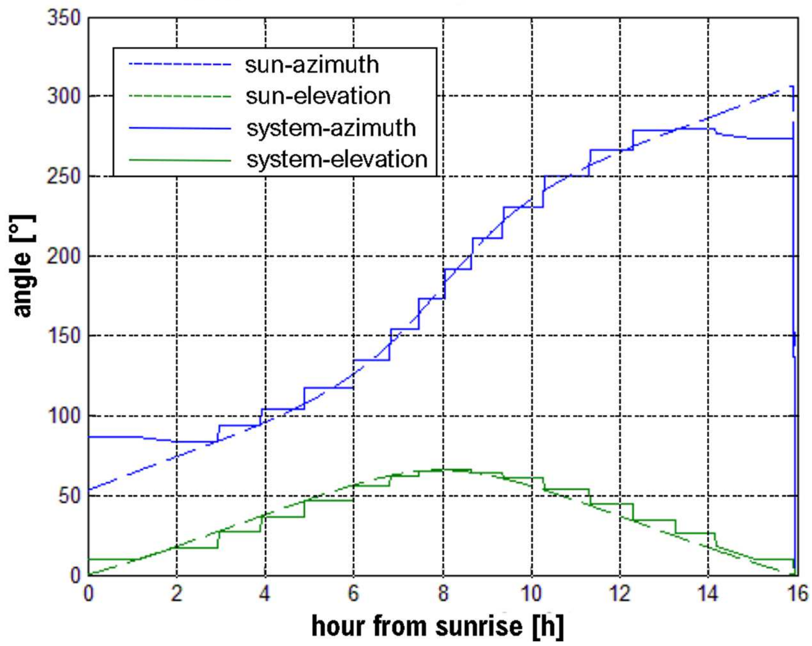

Figure 23. Daily course of system positioning—summer solstice.

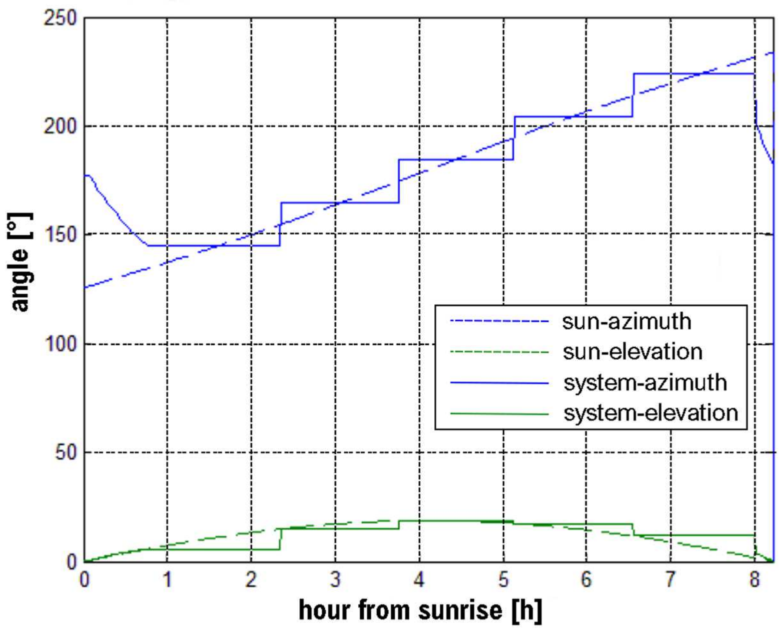

Figure 24. Daily course of system positioning—winter solstice.

By simulating individual daily trends, we can determine the gains for individual days of the year. However, here we are still talking about the potential generated power under the mentioned conditions and without considering the energy input to the positioning system. The annual course of the generated energy of the photovoltaic energy system in positioning and fixed implementation is shown in Figure 25.

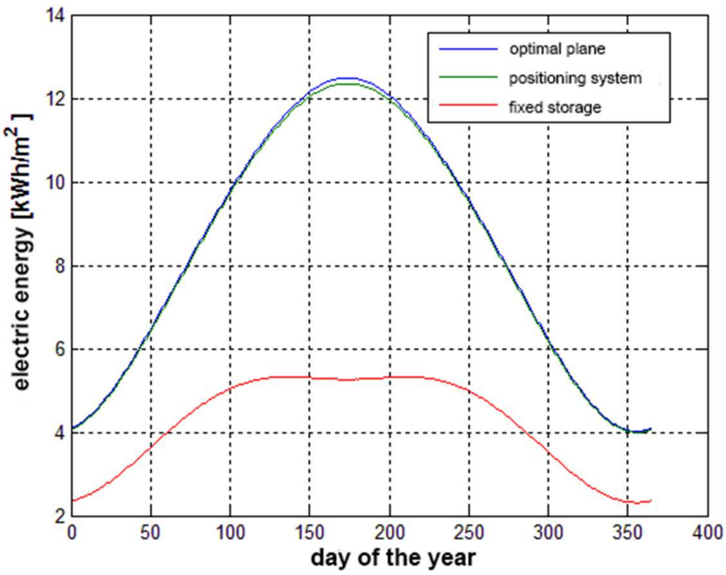

Figure 25. Potentially generated energy per day.

The potentially generated energy depicted in Figure 25 shows the benefit of the positioning device over fixed storage, with the positioning system ensuring the maximization of the potential amount of energy that can be produced. A significant increase can be observed in the summer season, due to the mentioned effects of the azimuth at sunrise and sunset, which is behind the plane of the fixed panel and there are significant deviations between the angles of the position of the Sun and the normal vector of the panel during the day. This problem is completely solved by the designed complex mechatronic system for positioning the photovoltaic panel.

However, to ensure the optimal position that maximizes the generated energy, the photovoltaic panel positioning system must spend a certain amount of energy on position changes during the year. We can express the electrical energy spent on the positioning of the system based on the knowledge of the drive system, as well as its operation time throughout the year. We can express the operating time based on the control frequency of stepper motors with a given nominal power, as well as the motors that operate the brake release mechanism on both axes. The parameters of the propulsion system are in Table 5. Based on these parameters, the results of the annual engine run analysis, as well as the calculated total energy input, are determined and summarized in Table 6.

Table 5. Parameters of the propulsion system.

Rated Engine Power	Rated Brake Power
8.96 W	15 W

Table 6. Evaluation of the energy deposit.

Number of Motor Steps	Drive Operation Time	Energy Input
837,219 steps/year	23.3 h/year	0.9 kWh/year

In the summary evaluation, the listed values are obtained from the analysis of the results and provide an illustrative example of the potential of using the positioning device in applications with one panel on the roofs of buildings. It should be noted that it is valid for the entire range of latitude as well as its surroundings, given the geographical location of Bratislava. Evaluation of the work results is summarized in Tables 7 and 8 with the consumption of both stepper motors. The visualization is not constantly displayed; it is only an information panel that starts when the user intervenes. It is similar a system add-on; therefore, its consumption is not included in the evaluation.

Table 7. Comprehensive results for a real photovoltaic panel (conversion efficiency: 17%, active area: 1.6 m^2).

Energy Falling on an Optimally Inclined Plane	Potential of Generated Energy—Positioning System	Potential of Generated Energy—Fixed System
3083 kWh/m^2/year	3057 kWh/m^2/year	1544 kWh/m^2/year

Table 8. General results.

Theoretical Generated Energy—Positioning System	Theoretical Generated Energy	Energy Deposit—Positioning System
832 kWh/m^2/year	420 kWh/m^2/year	0.9 kWh/m^2/year

The energy gain of the positioning system compared to the fixed system can be expressed as follows:

$$832 - 420 - 0.9 = 411.1 \text{ kWh/m}^2 \text{ per year (98\%)}.$$

The results show the theoretical value of the energy gain of the energy system using a positioning device compared to a fixed device. It must be noted, however, that it is given on the assumption of cloudless days and without the influence of diffuse radiation, which would reduce the total stated energy gain, because its influence is not included in the calculations. The achieved results indicate a significantly higher potential gain of generated energy compared to the commercially available solutions, e.g., [24,25].

All the requirements from Section 3.1 can be considered as fulfilled. Requirements 1 and 2 are fulfilled by the appropriate selection of the stepper motor. With the structural design solution, we ensured requirements 3, 4, 5, 6, 7, 9 and 10. By equipping the system with a tilt sensor, we also contributed to the verification of robustness (requirement 3). By choosing a PLC, the variability of the connection of several systems was ensured (requirement 8).

5. Conclusions

The result of the work is the design of a complex positioning device for photovoltaic panels that ensures the optimal inclination of the panel to achieve the maximum energy gain of the system. The proposal consists of a functional 3-D model of the structural solution in the CATIA program environment, a specific drive system in the form of real stepper motors that ensure optimal positioning based on the PLC control system, which is intended for the given proposal. This PLC did not have any influence on the energy gain calculations in the previous section.

The control algorithm that delivers the function of the positioning device is solved by a program written in the STEP7 environment, which ensures the operation of the entire mechatronic design, i.e., mainly the positioning of the photovoltaic panels to the optimal position. The course of the overall control, as well as the energy process, can be monitored and influenced through the visualization of the given process.

The visualization is solved using the WINCC program and provides the corresponding functions to the operator of the energy process. The conclusion of the work is the evaluation of the results achieved with the designed positioning system, ensuring the optimal gain of electrical energy. Based on the analyses, the results of the energy gain of the designed solution are determined against the energy gain from the fixed installation system, while the theoretical value of the gain of the designed positioning device is 98% compared to the fixed solution. However, the value would be smaller in practice, because the analysis does not include the influence of diffuse radiation. The presented complex design of the positioning PV system is believed to compete with the existing designs, for example see [26].

The next step in the future work would be to build a physical device, which we would test in real conditions and compare with the theoretical design.

Author Contributions: Conceptualization, F.Ž. and J.C.; methodology, J.C.; software, F.Ž.; validation, F.Ž., O.H. and E.K.; formal analysis, E.K. and D.R.; investigation, J.C.; resources, J.C., F.Ž. and D.R.; data curation, J.C. and E.K.; writing—original draft preparation, F.Ž. and J.C.; writing—review and editing, J.C. and D.R.; visualization, F.Ž.; supervision, J.C. and D.R.; project administration, J.C.; funding acquisition, J.C. All authors have read and agreed to the published version of the manuscript.

Funding: This research received no external funding.

Data Availability Statement: Data sharing is not applicable to this article.

Acknowledgments: The work has been supported by the Slovak Grant Agency VEGA 1/0107/22, KEGA 039STU-4/2021, Scientific Grant APVV-21-0125 and by the Operational Program Integrated Infrastructure for the project: "Research and development of the applicability of autonomous flying vehicles in the fight against the pandemic caused by COVID-19", Project no. 313011ATR9, co-financed by the European Regional Development Fund and by. Special thanks go to our student Ing. Miroslav Šimončič for his cooperation in the fulfilment of software tasks.

Conflicts of Interest: The authors declare no conflict of interest.

References

1. Our World in Data (2022)—Our World in Data based on BP Statistical Review of World Energy. Available online: https://ourworldindata.org/grapher/electricity-prod-source-stacked (accessed on 20 February 2023).
2. Saravanan, S.; Ramesh Babu, N. Maximum power point tracking algorithms for photovoltaic system—A review. *Renew. Sustain. Energy Rev.* **2016**, *57*, 192–204. [CrossRef]
3. Alboteanu, L.; Manolea, G.; Ravigan, F. Positioning systems for solar panels placed in isolated areas. *Ann. Univ. Craiova Electr. Eng.* **2006**. Available online: https://www.researchgate.net/publication/228860210_Positioning_systems_for_solar_panels_placed_in_isolated_areas/citations#fullTextFileContent (accessed on 20 February 2023).
4. Rhif, A. A Position Control Review for a Photovoltaic System: Dual Axis Sun Tracker. *IETE Tech. Rev.* **2011**, *28*, 479. [CrossRef]
5. Maish, A.B. Performance of a self-aligning solar array tracking controller. In Proceedings of the IEEE Photovoltaic Specialists Conference, Kissimimee, FL, USA, 21–25 May 1990.
6. Enslin, J.H.R. Maximum power point tracking: A cost saving necessity in solar systems. *Renew. Energy* **1992**, *2*, 543–549. [CrossRef]
7. Brown, D.G.; Stone, K.W. High accuracy/low cost tracking system for solar concentrators using a neural network. In Proceedings of the 28th Intersociety Energy Conversion Engineering Conference, Atlanta, GA, USA, 8–13 August 1993.
8. Kalogirou, S.A. Design and construction of a one-axis sun-tracking system. *Sol. Energy* **1996**, *57*, 465–469. [CrossRef]
9. Khalifa, A.N.; Al-Mutawalli, S.S. Effect of two-axis sun tracking on the performance of compound parabolic concentrators. *Energ. Convers. Manag.* **1998**, *39*, 1073–1079. [CrossRef]
10. Falbel, G.; Puig-Suari, J.; Peczalski, A. Sun oriented and powered, 3 axis and spin stabilized cubesats. In Proceedings of the IEEE Aerospace Conference, Big Sky, MT, USA, 9–16 March 2002.
11. Al-Mohamad, A. Efficiency improvements of photo-voltaic panels using a sun-tracking system. *Appl. Energy* **2004**, *79*, 345–354. [CrossRef]
12. Abdallah, S. The effect of using sun tracking systems on the voltage-current characteristics and power generation of flat plate photovoltaics. *Energy Convers. Manag.* **2004**, *45*, 1671–1679. [CrossRef]
13. Aiuchi, K.; Yoshida, K.; Katayama, Y.; Nakamura, M.; Nakamura, K. Sun tracking photo-sensor for solar thermal concentrating system. In Proceedings of the International Solar Energy Conference, Portland, OR, USA, 11–14 July 2004.
14. Blanco-Muriel, M.; Alarcón-Padilla, D.C.; López-Moratalla, T.; Lara-Coira, M. Computing the solar vector. *Sol. Energy* **2001**, *70*, 431–441. [CrossRef]
15. Abdallah, S.; Nijmeh, S. Two axes sun tracking system with PLC control. *Energy Convers. Manag.* **2004**, *45*, 1931–1939. [CrossRef]
16. Reda, I.; Andreas, A. Solar position algorithm for solar radiation applications. *Sol. Energy* **2004**, *76*, 577–589. [CrossRef]
17. Chen, F.; Feng, J.; Hong, Z. Digital sun sensor based on the optical vernier measuring principle. *Meas. Sci. Technol.* **2006**, *17*, 2494–2498. [CrossRef]
18. Chen, F.; Feng, J. Analogue sun sensor based on the optical nonlinear compensation measuring principle. *Meas. Sci. Technol.* **2007**, *18*, 2111–2115. [CrossRef]

19. Grena, R. An algorithm for the computation of the solar position. *Sol. Energy* **2008**, *82*, 462–470. [CrossRef]
20. Chong, K.K.; Wong, C.W. General formula for on-axis sun tracking system and its application in improving tracking accuracy of solar collector. *Sol. Energy* **2009**, *83*, 298–305. [CrossRef]
21. Gasparac, I.; Vrazic, M.; Petrovic, I. Expected and measured values of luminance sensors in dual-axis photovoltaic positioning system. In Proceedings of the 2nd IMEKO TC 11 International Symposium Metrological Infrastructure, Dubrovnik Riviera, Croatia, 15–17 June 2011.
22. Bahaidarah, H.M.; Tanweer, B.; Gandhidasan, P.; Rehman, S. A Combined Optical, Thermal and Electrical Performance Study of a V-Trough PV System—Experimental and Analytical Investigations. *Energies* **2015**, *8*, 2803–2827. [CrossRef]
23. Plachta, K. Autonomous Tracking Controller for Photovoltaic Systems Using Global Positioning System. In Proceedings of the 2018 IEEE International Conference on Environment and Electrical Engineering and 2018 IEEE Industrial and Commercial Power Systems Europe (EEEIC/I&CPS Europe), Palermo, Italy, 12–15 June 2018; pp. 1–5. [CrossRef]
24. Etop Alternative Energy, Active Construction for Photovoltaic Panels Sunflower-SF44V2P. Available online: https://etopalternativeenergy.sk/produkt/aktivna-konstrukcia-na-fotovoltaicke-panely-sunflower-sf44v2p/ (accessed on 12 February 2023).
25. Amazon, ECO-WORTHY Solar Panel Dual Axis Tracking System (Increase 40% Power) with Tracker Controller, Complete Solar Tracker Kit, Ideal for Different Solar Panels, for Yard/Farm/Field. Available online: https://www.amazon.com/ECO-WORTHY-Dual-Solar-Tracking-System/dp/B00JYAIS9W?th=1 (accessed on 12 February 2023).
26. Seme, S.; Štumberger, B.; Hadžiselimović, M.; Sredenšek, K. Solar Photovoltaic Tracking Systems for Electricity Generation: A Review. *Energies* **2020**, *13*, 4224. [CrossRef]
27. Lincot, D. The new paradigm of photovoltaics: From powering satellites to powering humanity. *Comptes Rendus Phys.* **2017**, *18*, 381–390. Available online: https://www.sciencedirect.com/science/article/pii/S1631070517300555 (accessed on 12 February 2023). [CrossRef]
28. Goetzberger, A.; Hebling, C.; Schock, H.-W. Photovoltaic materials, history, status and outlook. *Mater. Sci. Eng. R Rep.* **2003**, *40*, 381–390. Available online: https://www.sciencedirect.com/science/article/pii/S0927796X0200092X?casa_token=cbw-ZIYcs8wAAAAA:_g-vYcOOjCnDRxDySeJzYzBa-n7Ws8l_qbdq_1WwZokkG_dsIRxcP1wZ_v9DlBmPknP66T2ETw (accessed on 15 February 2023). [CrossRef]
29. Schaller, R.D.; Sykora, M.; Pietryga, J.M.; Klimov, V.I. Seven Excitons at a Cost of One: Redefining the Limits for Conversion Efficiency of Photons into Charge Carriers. *Nano Lett.* **2006**, *6*, 424–429. [CrossRef] [PubMed]
30. Alkasrawi, M.; Abdelsalam, E.; Alnawafah, H.; Almomani, F.; Tawalbeh, M.; Mousa, A. Integration of Solar Chimney Power Plant with Photovoltaic for Co-Cooling, Power Production, and Water Desalination. *Processes* **2021**, *9*, 2155. [CrossRef]
31. Welons, M. The Stefan-Boltzmann Law, College of Wooster Physics Department, Ohio, USA. 2007. Available online: https://physics.wooster.edu/wp-content/uploads/2021/08/Junior-IS-Thesis-Web_2007_Wellons.pdf (accessed on 15 February 2023).
32. Ramírez-Moreno, M.A.; González-Hernández, S.; Angulo-Brown, F. The role of the Stefan–Boltzmann law in the thermodynamic optimization of an n-Müser engine. *Phys. A Stat. Mech. Its Appl.* **2016**, *444*, 914–921. Available online: https://www.sciencedirect.com/science/article/pii/S037843711500953X (accessed on 15 February 2023). [CrossRef]
33. Honsberg, C.B.; Bowden, S.G. Photovoltaics Education Website. 2019. Available online: www.pveducation.org (accessed on 15 February 2023).
34. Wang, W. On the utilization and development of solar energy in Tibet. *E3S Web Conf.* **2021**, *329*. Available online: https://www.e3s-conferences.org/articles/e3sconf/abs/2021/105/e3sconf_gesd2021_01082/e3sconf_gesd2021_01082.html (accessed on 15 February 2023). [CrossRef]
35. Jenkins, J.H.; Fischbach, E.; Buncher, J.B.; Gruenwald, J.T.; Krause, D.E.; Mattes, J.J. Evidence of correlations between nuclear decay rates and Earth–Sun distance. *Astropart. Phys.* **2009**, *32*, 42–46. Available online: https://www.sciencedirect.com/science/article/pii/S092765050900084X?casa_token=V9abI0tmyM0AAAAA:nAFM-xdapi1Ry1AyPsQ_matymOchIklzvX4NT7JrTdJkra9CLvhvc-souZSA41pA45c7ocTONw (accessed on 18 February 2023). [CrossRef]
36. Murphy, D.M. Effect of Stratospheric Aerosols on Direct Sunlight and Implications for Concentrating Solar Power. *Environ. Sci. Technol.* **2009**, *43*, 2784–2786. [CrossRef] [PubMed]
37. Attivissimo, F.; Lanzolla, A.M.L.; Passaghe, D.; Paul, M.; Gregory, D.; Knox, A. Photovoltaic-thermoelectric modules: A feasibility study. In Proceedings of the 2014 IEEE International Instrumentation and Measurement Technology Conference (I2MTC) Proceedings, Montevideo, Uruguay, 12–15 May 2014; pp. 659–664.
38. ASC Chemistry for Life, Energy from the Sun. Available online: https://www.acs.org/content/acs/en/climatescience/energybalance/energyfromsun.html (accessed on 18 February 2023).
39. Wang, Q.; Li, S.; Jiang, F. Uncovering the impact of the COVID-19 pandemic on energy consumption: New insight from difference between pandemic-free scenario and actual electricity consumption in China. *J. Clean. Prod.* **2021**, *313*, 127897. [CrossRef]
40. Hofierka, J.; Cebecauer, T. Spatially distributed assessment of solar resources for energy applications in Slovakia. *Acta Fac. Studiorum Humanit. Nat. Univ. Prešoviensis. Prírodné Vedy Folia Geogr.* **2008**, *12*, 97–114.
41. Nijegorodov, N.; Luhanga, P.V.C. Air mass: Analytical and empirical treatment; an improved formula for air mass. *Renew. Energy* **1996**, *7*, 57–65. [CrossRef]
42. Li, Y.; He, C.; Zuo, L.; Zhao, F.; Zhan, L.; Li, X.; Xia, R.; Yip, H.; Li, C.; Liu, X.; et al. High-Performance Semi-Transparent Organic Photovoltaic Devices via Improving Absorbing Selectivity. *Adv. Energy Mater.* **2021**, *11*, 2003408. [CrossRef]

43. Landis, G.A.; Vo, T. Photovoltaic performance in the Venus environment. In Proceedings of the 2009 34th IEEE Photovoltaic Specialists Conference (PVSC), Philadelphia, PA, USA, 7–12 June 2009.
44. Karakaya, E. Finite Element Method for forecasting the diffusion of photovoltaic systems: Why and how? *Appl. Energy* **2016**, *163*, 464–475. [CrossRef]
45. Nayak, P.; Garcia-Belmonte, G.; Kahn, A.; Bisquert, J.; Cahen, D. Photovoltaic efficiency limits and material disorder. *Energy Environ. Sci.* **2012**, *5*, 6022–6039. [CrossRef]
46. Matuška, T. Solar thermal systems (MP 1.6.11). 2012. Available online: https://profesis.ckait.cz/dokumenty-ckait/mp-1-6/mp-1-6-11/ (accessed on 18 February 2023).
47. Reinders, A.; Verlinden, P.; van Sark, W. *Photovoltaic Solar Energy: From Fundamentals to Applications*; John Wiley & Sons: Hoboken, NJ, USA, 2017; p. 720.
48. Keevers, M.J.; Green, M.A. Absorption edge of silicon from solar cell spectral response measurements. *Appl. Phys. Lett.* **1995**, *66*, 174–176. [CrossRef]
49. Kira, M.; Jahnke, F.; Hoyer, W.; Koch, S.W. Quantum theory of spontaneous emission and coherent effects in semiconductor microstructures. *Prog. Quantum Electron.* **1999**, *23*, 189–279. [CrossRef]
50. University of Žilina, Faculty of Management Science and Informatics, Optoelectronic Components. Available online: https://www.kis.fri.uniza.sk/~ludo/e-Publikacia/elektronika/kap9/elektronika.html (accessed on 18 February 2023).
51. dos Santos, L.L.C.; Canha, L.N.; Bernardon, D.P. Projection of the diffusion of photovoltaic systems in residential low voltage consumers. *Renew. Energy* **2018**, *116*, 384–401. [CrossRef]
52. Mills, A.; Le Hunte, S. An overview of semiconductor photocatalysis. *J. Photochem. Photobiol. A Chem.* **1997**, *108*, 1–35. [CrossRef]
53. Pleskov, Y. *Semiconductor Photoelectrochemistry*; Springer: New York, NY, USA, 1986; ISBN 978-1-4684-9080-0.
54. Benda, V.; Cerna, L. A Note on Limits and Trends in PV Cells and Modules. *Appl. Sci.* **2022**, *12*, 3363. [CrossRef]
55. Obukhov, S.G.; Plotnikov, I.A.; Sheryazov, S.K. Methods of effective use of solar power system. In Proceedings of the 2016 2nd International Conference on Industrial Engineering, Applications and Manufacturing (ICIEAM), Chelyabinsk, Russia, 19–20 May 2016.
56. Emery, K.A. Solar simulators and I–V measurement methods. *Sol. Cells* **1986**, *18*, 251–260. [CrossRef]
57. Kang, R.; Jeong, T.; Lee, B. Lead-Free Perovskite and Improved Processes and Techniques for Creating Future Photovoltaic Cell to Aid Green Mobility. 2022. Available online: https://www.intechopen.com/online-first/84068 (accessed on 18 February 2023).
58. Jäger-Waldau, A. *Overview of the Global PV Industry, Reference Module in Earth Systems and Environmental Sciences*; Elsevier: Amsterdam, The Netherlands, 2013; ISBN 9780124095489.
59. Alternative Energy Tutorials, Solar Panel Orientation—PV Solar Panel Orientation and Positioning. 2015. Available online: https://www.alternative-energy-tutorials.com/solar-power/solar-panel-orientation.html (accessed on 18 February 2023).
60. Walraven, R. Calculating the position of the Sun. *Sol. Energy* **1978**, *20*, 393–397. [CrossRef]
61. Energy Education, Solar Panel Orientation. 2018. Available online: https://energyeducation.ca/wiki/index.php?title=Solar_panel_orientation&oldid=6109 (accessed on 21 February 2023).
62. Marsh, J. What's the Best Direction and Angle for My Solar Panels? Available online: https://news.energysage.com/solar-panel-performance-orientation-angle/ (accessed on 21 February 2023).
63. Božiková, M.; Bilčík, M.; Madola, V.; Szabóová, T.; Kubik, Ľ.; Lendelová, J.; Cviklovič, V. The Effect of Azimuth and Tilt Angle Changes on the Energy Balance of Photovoltaic System Installed in the Southern Slovakia Region. *Appl. Sci.* **2021**, *11*, 8998. [CrossRef]
64. Catia. Available online: https://www.3ds.com/products-services/catia/ (accessed on 21 February 2023).
65. MSC Adams. Available online: https://hexagon.com/products/product-groups/computer-aided-engineering-software/adams (accessed on 23 February 2023).
66. Matlab. Available online: https://www.mathworks.com/products/matlab.html (accessed on 21 February 2023).
67. Siemens Simatic Step7. Available online: https://new.siemens.com/global/en/products/automation/industry-software/automation-software/tia-portal/software/step7-tia-portal.html (accessed on 23 February 2023).
68. Siemens WinCC. Available online: https://new.siemens.com/global/en/products/automation/industry-software/automation-software/scada/simatic-wincc-v7.html (accessed on 23 February 2023).